國立交通大學

電信工程學系

碩士論文

新型態多天線系統綜合分析

New Composite Analysis Strategies of Multiple Antenna Systems

研 究 生：謝博全 (Po-Chuan Hsieh)

指導教授：陳富強 博士 (Dr. Fu-Chiarng Chen)

中 華 民 國 九 十 六 年 九 月

新型態多天線系統綜合分析

New Composite Analysis Strategies of Multiple Antenna Systems

研 究 生：謝博全　　Student：Po-Chuan Hsieh

指導教授：陳富強　博士　　Advisor：Dr. Fu-Chiarng Chen

國 立 交 通 大 學

電 信 工 程 學 系

碩 士 論 文

A Thesis

Submitted to Department of Communication Engineering
College of Electrical Engineering and Computer Science
National Chiao Tung University
in partial Fulfillment of the Requirements
for the Degree of
Master of Science
in
Communication Engineering
August 2007
Hsinchu, Taiwan, Republic of China

中 華 民 國 九 十 六 年 九 月

新型態多天線系統綜合分析

學生：謝博全　　指導教授：陳富強 博士

國立交通大學電信工程學系碩士班

摘要

在本論文中，我們提出了兩組新型評估多天線系統效能的電磁分析。第一項是新型天線空間相關係數(Antenna Spatial Correlation)的計算方法，第二項則是結合全主動反射係數(Total Active Reflection Coefficient)的輻射效率(Radiation Efficiency)分析方法。論文中的所有個案討論將以一對偶極天線做為分析基準。

首先，我們提出了一組新型態的天線空間相關係數表式方法。新型天線空間相關係數計算方式擁有以下的優勢。首先，新型態的計算方法將整體的計算參數化，分離了天線場型、天線電路的耦合效應(Mutual Coupling Effect)以及入射角度的機率分佈函數(Angle-of-Arrival Probability Distribution Function)三組參數進行計算，如此的計算方式可以將三者分別對相關係數的影響進行檢驗，有利於對於整體效能的分析評估，並可節省計算受到耦合效應影響的天線場型的時間。再者，在進行關於入射角度的機率分佈的相關計算中，我們提出了計算任意入射角度分佈的相關係數積分近似方法，此方法可以有效降低計算複雜度。

此外，我們也提出了一組新的結合全主動反射係數的輻射效率分析方式。他能分析輻射效率如何隨著天線埠饋入不同相位訊號時有所改變，相對也更適合於多天線系統的分析。運用這一組分析方法，我們也進一步研究不同的天線匹配網路如何影響輻射效率以及天線空間相關係數。

New Composite Analysis Strategies of Multiple Antenna Systems

Student: Po-Chuan Hsieh Advisor: Dr. Fu-Chiarng Chen

Department of Communication Engineering
National Chiao Tung University

Abstract

In the thesis, we propose two new electromagnetic analysis strategies to evaluate the performance of multiple antenna systems. The first is a new antenna spatial correlation formulation, and the other is a new analysis strategy of radiation efficiency combined with total active reflection coefficient (TARC). All case studies are simulated using a dipole pair as the benchmark.

The new proposed antenna spatial correlation formulation is presented in the parameterized manner. The formulation separates the isolated antenna pattern, the mutual coupling effect between antennas, and the probability distribution function (PDF) of Angle-of-Arrival (AoA) to calculate the correlation coefficient. Such formulation not only benefits the analysis of the performance of the whole antenna system but also saves the computation time of the distorted antenna patterns which result from the mutual coupling effect. Moreover, we provide an approximate spatial correlation formulation which is suitable for arbitrary AoA scenarios and can be incorporated in our parameterized correlation formulation. This approximation formulation can effectively reduce computation complexity.

We further propose a new analysis strategy of radiation efficiency combined with TARC technique. It evaluates how the radiation efficiency may change when the antenna ports excite signals with different phases. Besides, with this new technique, we also investigate how different antenna termination networks influence the radiation efficiency and antenna spatial correlation.

Acknowledgements

I would like to dedicate the thesis to those all having given me assistance through these two important years in my life.

Thank my advisor, Dr. Fu-Chiarng Chen, for all the considerate care, enlightened discussion and valuable advice. Sincere thankfulness is also overwhelmed in my heart for my elder fellow members A-Nan, YTK, Hao, Monkey, and A-P, have brought me so much knowledge and academic inspiration so that I can keep my research in correct direction. I learned how to conduct a survey from them above, and that would be the most precious present for me. Furthermore, without my dearest fellow colleagues including Koo-A, LK, A-Pen and all younger lab members, I don't think I am lucky enough to lead such a great life in these two years with so many unforgettable memories. They really enrich my life!

Finally, I can never overemphasize my gratitude for my family. I am not who I am without their irreplaceable love and support.

Contents

Figure Captions

Table Captions

Acronym Glossary

2-D	two-dimensional
2G	second-generation
3-D	three-dimensional
3G	third-generation
AoA	angle-of-arrival
AS	angular-spread
EM	electromagnetic
MIMO	multiple-input multiple-output
NLOS	non line-of-sight
OFDM	orthogonal frequency-division multiplexing
PDF	probability distribution function
RSM	radiation swing margin
SINR	signal-interference-noise ratio
STBC	space time block coding
TARC	total active reflection coefficient
UWB	ultra-wideband
WiMAX	worldwide interoperability for microwave access
WLAN	wireless local area network
XPR	cross polarization ratio

Chapter 1

Introduction

In recent years, the magnificent progress of wireless communication has boosted the rapid development of the whole communication industry. Because of the even firmer connection with our daily lives, wireless communication actually has changed the way we live. Standards such as the second-generation (2G) mobile communication, bluetooth and wireless local area network (WLAN) have been extensively implemented since a decade ago. Moreover, some newly-suggested technologies like the third-generation (3G) systems, ultra-wideband (UWB), worldwide interoperability for microwave access (WiMAX) blossom on the standard platform of the wireless communication. Telecom and datacom have come to aim at combining with each other in an even higher speed. Mainly owning to the variety of the wireless standards, it has become an essential issue and technology to make the best use of the limited frequency spectrum efficiently and achieve high information quality.

1.1 Motivation

The concept of multiple antenna technology has offered a solution scheme which can reach the goal of high-quality communications. From a theoretical perspective, multiple antenna transmission and reception techniques are well known in communication engineering [1] and envisioned as the solution for next generation

broadband communication systems. It is acknowledged for the potential benefits for increasing the coverage, capacity, and data rates of the wireless communication systems.

Incorporating multiple antenna technology into portable wireless devices means that multiple antennas are set in the limited spacing of small devices and impacts system performance. The spatial propagating channel and the characteristics of antennas are considered two most concerned factors which actually impact system performance, and antenna spatial correlation is therefore suggested the composite representation of these two factors for evaluating the performance of the multiple antenna system. In previous works which will be reviewed in the next chapter, antenna spatial correlation is defined as the Hermitian product of the far-field patterns of two antenna elements which may moreover take the probability distribution function (PDF) of angle-of-arrival (AoA) into consideration for the expectation value of the antenna spatial correlation coefficient.

In addition to antenna spatial correlation, radiation efficiency is another topic when referring to the performance of multiple antenna systems. Realizing multiple antenna systems in radiation channels becomes challenging because of the unavoidable mutual coupling effect between multiple antennas. Mutual coupling effect not only distorts the antenna far-field patterns but also has great impact on how much power can radiate without reflection resulting from impedance mismatch and absorption by adjacent antenna elements.

1.2 Purpose

In the thesis, we propose two new electromagnetic analysis strategies to evaluate the performance of multiple antenna systems. The first is a new antenna spatial

correlation formulation, and the other is a new analysis strategy of radiation efficiency combined with total active reflection coefficient (TARC). This investigation is especially more valuable when the system operates in the transmit mode. The new antenna spatial correlation formulation not only effectively reduces computation complexity without sacrificing accuracy but also offers a more detailed analysis presented in the parameterized manner. Moreover, the new suggested analysis of radiation efficiency combined with TARC evaluates how the radiation efficiency may change when the antenna ports excite signals with different phases.

1.3 Organization

This thesis is organized as follows. In Chapter 2, the overview of multiple antenna systems is introduced, and the two analysis strategies of multiple antenna systems including complex antenna spatial correlation and radiation efficiency are reviewed for the further investigation in the following chapters. In Chapter 3, the two-dimensional (2-D) approximate antenna spatial correlation without mutual coupling is first proposed, and then the 2-D and 3-D antenna spatial correlation formulation incorporating antenna mutual coupling is further presented in the following sections in this chapter. Chapter 4 describes the new proposed TARC-based radiation efficiency, and we also provide investigations of impact of different termination networks on antenna spatial correlation and radiation efficiency based on the newly-proposed analysis strategy. Finally, we draw concluding remarks in Chapter 5.

Chapter 2

Fundamental Theory of Multiple Antenna Systems

Wireless communication systems are becoming more complex to cope with the growing demand for more data rates, wider coverage, larger capacity objectives, as well as exciting new wireless applications. Multiple antenna systems have great potential in reaching these specifications and overcoming the impairments of these systems by exploiting the spatial domain to reduce the interference of the undesired signals, extend the coverage of wireless networks, increase capacity, and reach high information throughput. In this chapter, we will first review the multiple antenna systems and especially focus on the detailed classification of different multiple antenna system schemes. Based on the overall introduction of multiple antenna systems, we further introduce two important parameters for the gauge of the performance of multiple antenna systems. The first one is the antenna spatial correlation where we will review several definitions of antenna spatial correlation in the second section of this chapter. The second parameter is the radiation efficiency which will be fully discussed based on the general definition and shown why it plays an important role in multiple antenna systems. Finally, because the case studies we provide in the whole thesis are simulated using a dipole pair, the dipole antenna is briefly introduced as well in the final section of the chapter.

2.1 Overview of Multiple Antenna Systems

It is a truth that current technologies have maximized the employment of temporal and spectral techniques to improve capacity and data speeds. There is still an additional degree of freedom left for full utilization, namely space [2]. Making use of space means multiple antenna elements are arranged together in the required manner. The concepts of multiple antenna technology that originate from decade ago are substantially beneficial in the wireless communication systems. Multiple antenna systems have developed into several appearances for implementation, and we further introduce all of them briefly and summarize their benefits respectively as follows.

· Beamforming: The concept of this multiple antenna system originates from the conventional phased antenna array. The radiation pattern of the phased antenna array system can be controlled by feeding different signal phase delays and antenna element spacing [3]. With a specific feeding network, the total pattern of the array can be directed to the desired direction. On basis of this concept, beamforming is developed as one main multiple antenna strategy. There are two general types of beamforming, namely, fixed beamforming and adaptive beamforming. The main advantage of adaptive beamforming antenna systems over fixed beamforming antenna systems is the ability to steer beams toward desired signals and nulls toward interfering signals while the fixed beamforming can only radiate/receive signals at specific directions [4]. Beamforming offers interference rejection, antenna gain and spatial filtering, which have the equivalent effects of improving signal-interference-noise ratio (SINR) as well.

· Diversity: The concept of diversity comes from the fact that when multiple replicas or multipath effects of the transmitted signal fade independently as they go through channels, the probability of a deep fade happening in all propagating routes

are greatly reduced. Diversity techniques provide a diversity gain or a reduction in the margin required to overcome fading. Several antenna schemes are proposed to create the diversified channels to achieve the diversity gain, including polarization and spatial diversity. Polarization diversity exploits antenna with orthogonal polarizations to achieve the performance of high diversity gain. Spatial diversity systems are designed such that the signals at the different antennas of the receiver have low cross correlation with maximum gain achieved for uncorrelated signals. Moreover, transmit diversity such as Alamouti's space time block coding (STBC) [5] can improve the quality of signals by proving data with multiple independent coded streams. Spatial diversity is supposed to provide diversity gain and prevent fade margin.

· Spatial Multiplexing: Spatial multiplexing is supported to urge forward the data rates and throughput to an even higher level. Multiple data streams are transmitted to multiple antennas with this spatial strategy. Moreover, if the receiver end is also set up with multiple antennas and signals are with sufficiently different spatial signatures, it can separate data streams to reach the goal of high data rate compared to the single-antenna communication systems. Spatial multiplexing is therefore considered very powerful for increasing channel capacity. One thing to emphasize is this spatial technique works under 1) multiple scattering rich environments and 2) enough good signal-to-noise-ratio (SNR).

The above three multiple antenna systems all involve complex vectors and matrix operation on signals, and sometimes can be generally called the family of multiple-input multiple-output (MIMO) antenna technology for these three systems share the same characteristic of multiple antennas. MIMO used to only indicate the diversity and spatial multiplexing techniques. However, with the advance of combining all three techniques into a total communication solution, MIMO now represents the systems which exploit many antennas. For example, spatial

multiplexing or diversity can also be combined with beamforming when the channel is known at the transmitter, and the definition of MIMO can be broadened in an extensive manner as a result. Furthermore, a combination of MIMO with orthogonal frequency division multiplexing (OFDM) is promising for frequency selective channels, high spectral efficiency, and reduction of circuit complexity.

No matter what kind of MIMO technology is implemented, antenna spatial correlation and radiation efficiency have always been very important parameters for evaluating the MIMO systems. Different multiple antenna transmission methods set different requirements on the antenna set up in addition to the number of antenna elements. Generally, the beamforming technique usually needs the antenna setups with spatial correlation as high as possible, while the diversity and spatial multiplexing techniques on the contrary demand uncorrelated antenna setups. Radiation efficiency is another issue we need to take care of because power consumption and how much power will radiate are concerned topics especially in small terminals like mobile phones. In the following two sections, we will review the definitions of these parameters.

2.2 Antenna Spatial Correlation

Signal fading due to multiple scattering effect is the dominant drawback happening in the wireless communication. Therefore, multiple antennas are proved to provide diversity, and the performance of the multiple antennas is determined by the spatial correlation between antennas. The first discussed spatial antenna correlation was proposed by W. C. Jakes [6]. Consider a plane wave arriving at an array from azimuth angle Φ with respect to the normal bisecting two sources a distance d apart, and the spatial correlation between two sources can be determined as

$$\rho(d) = \int_{-\pi}^{\pi} \exp(j2\pi \frac{d}{\lambda} \sin(\phi)) p_{\phi}(\phi) d\phi \qquad (2.1)$$

where λ is the wavelength and $p_\Phi(\Phi)$ is the azimuth angular probability distribution function. The most special case is when $p_\Phi(\Phi)=1/2\pi$ which is called the Clarke's model scenario [7], the antenna spatial correlation has a closed form well-known as the Bessel function [8]. Based on (2.1), several works on spatial correlation has relied on numerical integration to evaluate the correlation coefficient between two sources based on different azimuth angular probability distribution functions [9-10]. The author in [11] especially discussed and derived simple generalized formula for spatial correlation and showed a good approximation for spatial correlation for small angular-spread (AS) angular distributions.

The above definitions of antenna spatial correlation only take the signal phase and the angular PDF of the incoming waves in azimuth plane. Therefore, the antenna spatial correlation including antenna patterns and mutual coupling effect was further proposed in the literature. There were two main categories for the antenna spatial correlation including antenna patterns and mutual coupling effect. The first is the parameterized correlation formulation which describes the correlation in impedance or scattering matrix, and the second is the correlation formulation generally defined as the Hermitian product of the far-field patterns of two antenna elements.

· Parameterized Formulation: In [12], W. Wasylkiwskyj and W. K. Kahn suggested the antenna spatial correlation as

$$\rho_{12}(d) = \frac{R_{12}}{\sqrt{R_{11}R_{22}}} \qquad (2.2)$$

where R_{ii} is the self impedances of the i-th antenna, and R_{ij} is the mutual impedance between the i-th and j-th antennas. What needs to be noticed is this formulation is suitable for the minimum scattering antenna theory only. Moreover, the authors in [13]

proposed exact representation of antenna envelope correlation in terms of scattering parameter description under the assumption of uniformly incoming waves as listed in Equation (2.3).

$$\rho_{env} = \left|\rho_{12}\right|^2 = \frac{\left|S_{11}^{*}S_{12} + S_{21}^{*}S_{22}\right|^2}{\left(1-\left|S_{11}\right|^2-\left|S_{12}\right|^2\right)\left(1-\left|S_{22}\right|^2-\left|S_{21}\right|^2\right)} \tag{2.3}$$

· Pattern Multiplication: This is the most direct but also the most complex definition. R. G. Vaughan and J. B. Andersen proposed in [8] that the spatial correlation is given by

$$\rho_{12} = \frac{\iint_{\Omega}\left[P_1(\phi,\theta)\bullet P_2(\phi,\theta)\right]d\Omega}{\sqrt{\iint_{\Omega}\left|P_1(\phi,\theta)\right|^2 d\Omega \iint_{\Omega}\left|P_2(\phi,\theta)\right|^2 d\Omega}} \tag{2.4}$$

where • denotes the Hermitian product and P means the antenna pattern. Moreover, C. Waldschmidt and W. Wiesbeck further suggested a more general spatial correlation as [14]

$$\rho_{12} = \frac{R_{12}}{\sqrt{\sigma_1^2\sigma_2^2}} \tag{2.5}$$

where

$$R_{12} = \int_0^{\pi}\int_0^{2\pi}\begin{bmatrix} E_{\theta 1}(\phi,\theta)\cdot E_{\theta 2}(\phi,\theta)\cdot p_{\theta}(\phi,\theta) \\ +E_{\phi 1}(\phi,\theta)\cdot E_{\phi 2}(\phi,\theta)\cdot p_{\phi}(\phi,\theta)\end{bmatrix}\sin\theta d\theta d\phi \quad \text{and}$$

$$\sigma_i^2 = \int_0^{\pi}\int_0^{2\pi}\begin{bmatrix} \left|E_{\theta i}(\phi,\theta)\right|^2\cdot p_{\theta}(\phi,\theta) \\ +\left|E_{\phi i}(\phi,\theta)\right|^2\cdot p_{\phi}(\phi,\theta)\end{bmatrix}\sin\theta d\theta d\phi \tag{2.6}$$

E is the far-field E antenna patterns, p(Φ,θ) means the AoA distribution of interest, and the subscript Φ/θ denotes the field polarization for both AoA distribution and antenna patterns.

Compared with the pattern multiplication, the correlation represented in parameter manner encloses the total radiation field of antennas and extracts the

correlation from the principle of energy conservation, which will in turn lose some important information originally existing in the integral equations. As a consequence, the spatial correlation in Equation (2.5) is considered the most general correlation formulation so far because it takes all the possible factors into consideration to calculate the correlation coefficient.

2.3 Radiation Efficiency

For single antenna case, the total antenna radiation efficiency is used to take into account losses at the input terminals and within the antenna configurations. Such losses are listed as follows and refer to Figure 2.1 [3].

In general, the overall efficiency can be written as

$$e_o = e_r e_c e_d = e_r e_{cd} = e_{cd}\left(1 - |\Gamma|^2\right) \tag{2.7}$$

where

e_o = total efficiency,

e_r = reflection (mismatch) efficiency,

e_c = conduction efficiency,

e_d = dielectric efficiency,

e_{cd} = conduction and dielectric efficiency,

Γ = voltage reflection coefficient at the input terminals of the antenna

$= \dfrac{Z_{in} - Z_0}{Z_{in} + Z_0}$ where Z_{in} is the antenna input impedance and Z_0 is the characteristic impedance of the transmission line.

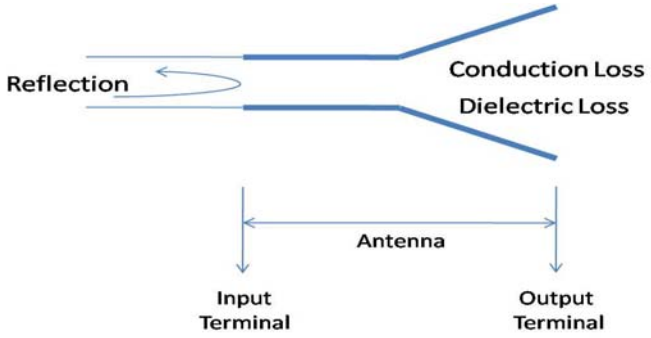

Figure 2.1 Reflection, conduction, and dielectric losses.

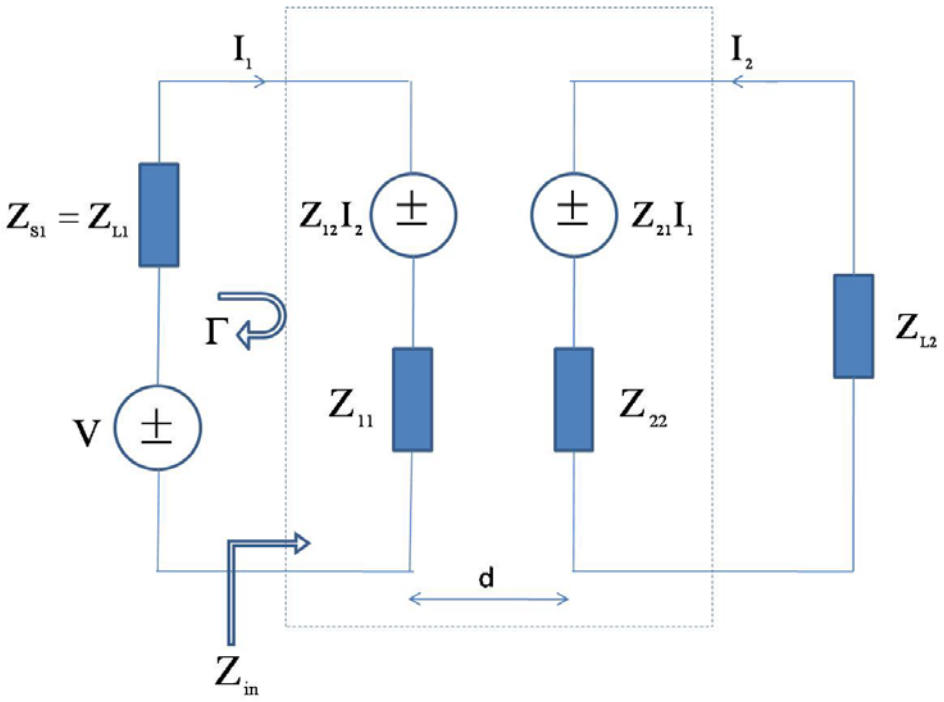

Figure 2.2 The equivalent circuit of an antenna pair in transmit mode.

We in turn introduce the general definition of radiation efficiency in multiple antenna systems [15]. The radiation efficiency is most conveniently defined and computed in the transmit mode by implementing the equivalent circuit shown in Figure 2.2. The voltage source V and source impedance Z_{S1} show the excitation of the antenna port 1, and the load impedance Z_{L2} is the termination at the second antenna port. Z_{12} is the mutual impedance which can describe the mutual coupling effect between two antennas. One thing to be mentioned is this equivalent circuit is constructed based on the antenna pair with identical structure, and Z_{11}=Z_{22} and Z_{12}=Z_{21} accordingly.

The equivalent circuit in Figure 2.2 can be used to calculate the input impedance Z_{in}, which can in turn calculate the voltage reflection coefficient Γ. We can determine the input impedance Z_{in} as

$$Z_{in} = Z_{11} + \frac{Z_{12} I_2}{I_1} \tag{2.8}$$

Equation (2.8) can be transformed using the circuit loop which represents the equivalent circuit of antenna 2 by

$$I_2 = \frac{-Z_{12}}{Z_{22} + Z_{L2}} I_1 \tag{2.9}$$

Then, we can finally determine the input impedance Z_{in} as

$$Z_{in} = Z_{11} - \frac{Z_{12}^2}{Z_{22} + Z_{L2}} \tag{2.10}$$

The total power leaving antenna 1 is shown as $P_{Zin}=\text{Real}\{Z_{in}\}|I_1|^2$, and the power which will be absorbed by Z_{L2} via mutual coupling effect and cause reduction of radiation power is $P_{ZL2}=\text{Real}\{Z_{L2}\}|I_2|^2$. The difference between P_{Zin} and P_{ZL2} is called the radiation power P_{rad}, i.e., $P_{rad}= P_{Zin}- P_{ZL2}$. Therefore, the radiation efficiency e_{rad} which is also defined in [3] can be derived as

$$e_{rad} = e_{refl} e_{Z_{L2}} \tag{2.11}$$

where

$$e_{refl} = 1 - |\Gamma|^2 \text{ and } \Gamma = \frac{Z_{in} - Z_0}{Z_{in} + Z_0} \tag{2.12}$$

$$e_{ZL2} = 1 - \frac{\text{Real}\{Z_{L2}\}|I_2|^2}{\text{Real}\{Z_{in}\}|I_1|^2} \tag{2.13}$$

The radiation efficiency is the composite power efficiency representation for it includes not only the reflection caused by input mismatch of the excitation port but also the power absorption resulting from the termination at the other unexcited antenna branch.

2.4 Dipole Antenna

Because the case studies we provide in the whole thesis are simulated using a

dipole pair, the dipole antenna is briefly introduced in this section. The dipole antenna is the most general antenna structure, and the current distribution on the dipole usually assumes the antenna is center-fed and the current vanishes at the end points. Moreover, to reduce the mathematical complexities, the diameter of the dipole is ideally much thinner than the wavelength of the operating frequency.

With the above assumptions, the current distribution can be approximately written as

$$I(z)=\begin{cases}\hat{a}_z I_0 \sin\left[k\left(\frac{l}{2}-z\right)\right], & 0\le z\le\frac{l}{2}\\ \hat{a}_z I_0 \sin\left[k\left(\frac{l}{2}+z\right)\right], & -\frac{l}{2}\le z\le 0\end{cases} \tag{2.14}$$

where I_o is the maximum current occurring at the center-fed point, and k is the phase constant in the free space. After the far-field approximations and integration of all

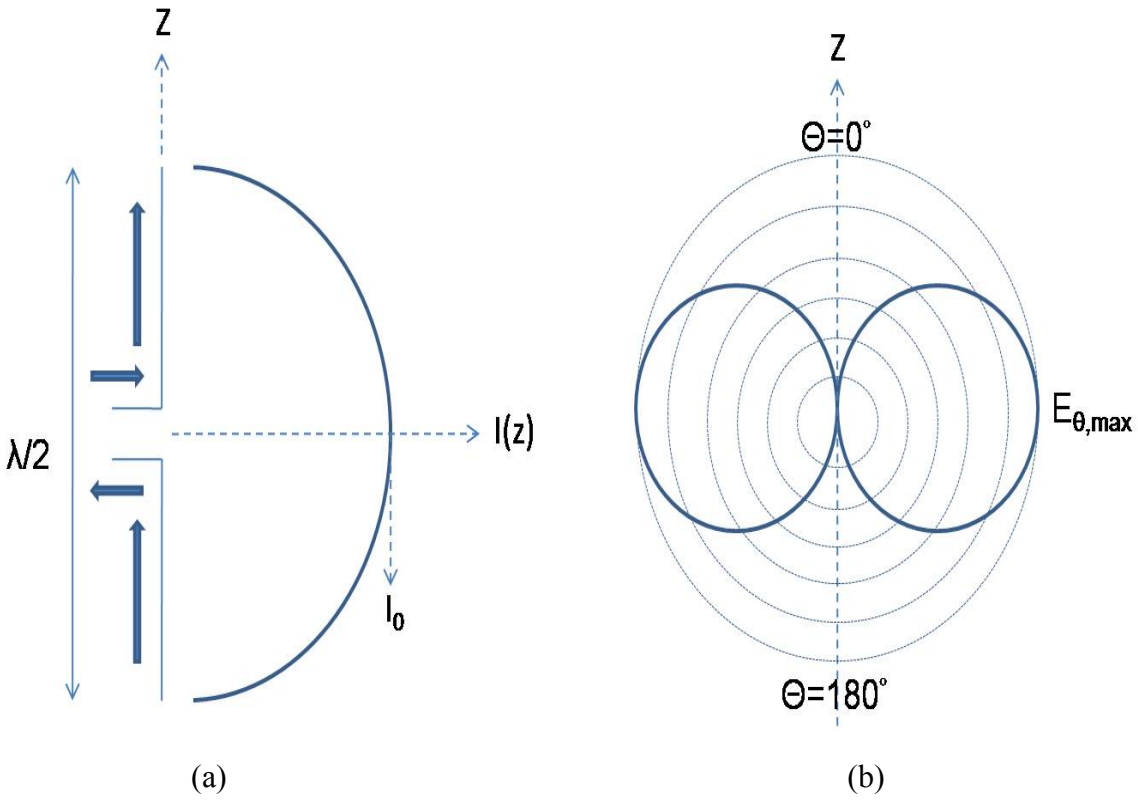

(a) (b)

Figure 2.3 (a) The λ/2 dipole and (b) the E_θ pattern in theta plane (Φ=0°).

the infinitesimal elements, the far-field E_θ pattern takes the form of

$$E_\theta = j\eta \frac{I_0 e^{-jkr}}{2\pi r}\left[\frac{\cos\left(\frac{kl}{2}\cos\theta\right)-\cos\left(\frac{kl}{2}\right)}{\sin\theta}\right] \tag{2.15}$$

In the similar manner, the total H_Φ component can be written as

$$H_\phi = \frac{E_\theta}{\eta} = j\frac{I_0 e^{-jkr}}{2\pi r}\left[\frac{\cos\left(\frac{kl}{2}\cos\theta\right)-\cos\left(\frac{kl}{2}\right)}{\sin\theta}\right] \tag{2.16}$$

One of the most commonly used type is the half-wavelength (l=λ/2) dipole for its matching to the transmission line is simplified especially at resonance. By letting l=λ/2, Equations (2.15) and (2.16) can reduce to

$$E_\theta = j\eta \frac{I_0 e^{-jkr}}{2\pi r}\left[\frac{\cos\left(\frac{\pi}{2}\cos\theta\right)}{\sin\theta}\right] \tag{2.17}$$

$$H_\phi = \frac{E_\theta}{\eta} = j\frac{I_0 e^{-jkr}}{2\pi r}\left[\frac{\cos\left(\frac{\pi}{2}\cos\theta\right)}{\sin\theta}\right] \tag{2.18}$$

The current distribution of the half-wavelength dipole and the theta-plane E-field pattern is plotted in Figure 2.3, and Z_{in}=73+42j computed from the induced EMF method [16]. We need to notice that we assume the diameter of the dipole is ideally much thinner than the wavelength of the operating frequency, and only E_θ and H_Φ fields exist. However, in the following chapters, E_Φ and H_θ fields also exist in the simulation results since the diameter of the dipole cannot be in ideally thin manner.

Chapter 3

A New Spatial Correlation Formulation of Arbitrary AoA Scenarios

Signal fading due to multiple scattering effect is the dominant drawback happening in the wireless communication. Therefore, multiple antennas are proved to provide diversity, and the performance of the multiple antennas is determined by the spatial correlation between antennas. In this chapter, we will discuss this parameter including the AoA distributions of the spatial channel and the physical configurations of multiple antenna structures. We first introduce the 2-D approximate spatial correlation formulation and our proposed approximate spatial correlation formulation of arbitrary AoA scenarios in Section 3.1. Based on the proposed formulation, Section 3.2 further introduces the 2-D spatial correlation combining with antenna patterns distorted by the mutual coupling effect based on the spatial correlation proposed in [17]. Finally, in Section 3.3, we derive a 3-D spatial correlation incorporating antenna mutual coupling in the parameterized manner. The new antenna spatial correlation formulation not only effectively reduces computation complexity without sacrificing accuracy but also offers a more detailed analysis presented in the parameterized manner. Again, we emphasize all the simulation results are provided using a dipole pair as the benchmark.

3.1 2-D Approximate Spatial Correlation Formulation of Arbitrary AoA Scenarios

3.1.1 Spatial Correlation of Small Angular Spread AoA Scenarios

The spatial channel model is different from the traditional propagation model which does not take into consideration the spatial angular distribution. A channel model that simultaneously characterizes the AoAs of multipath components is called the spatial channel model [18], and different phi-plane AoA PDFs have been proposed in the literature [19].

With a given AoA scenario, we may substitute it into the spatial correlation. In [11], the author presented the approximate spatial correlation which is suitable for small angular-spread AoA distribution. Consider a plane wave arriving at an array from azimuth angle Φ with respect to the normal bisecting two sources a distance d apart, and the spatial correlation between two sources can be determined as

$$\rho(d) = \int_{-\pi}^{\pi} \exp(j2\pi \frac{d}{\lambda} \sin(\phi)) p_{\phi}(\phi) d\phi \tag{3.1}$$

where λ is the wavelength and $p_{\Phi}(\Phi)$ is the azimuth angular PDF. If the angular energy is a Gaussian distribution, AoA distribution $p_{\Phi}(\Phi)$ can be represented as

$$p_{\phi}(\phi) = \frac{1}{\sqrt{2\pi}\sigma} \exp\left\{ -\frac{(\phi - \phi_0)^2}{2\sigma^2} \right\} \tag{3.2}$$

where σ is the standard deviation of the distribution and Φ_0 is the mean angle of the AoA distribution. Substitute Equation (3.2) into Equation (3.1) and make a change of variables, and the spatial correlation is given by

$$\rho(d)=\frac{1}{\sqrt{2\pi}}\int_{-\pi}^{\pi}\exp\left\{j2\pi\frac{d}{\lambda}\sin(\sigma z+\phi_0)\right\}\exp\left\{-\frac{z^2}{2}\right\}dz \qquad (3.3)$$

Under the assumption of small σz over the integration range, Equation (3.3) can be approximated as

$$\rho(d)=\exp\left\{j\frac{2\pi d}{\lambda}\sin(\phi_0)\right\}\exp\left\{-\frac{\left(\frac{2\pi d}{\lambda}\sigma\cos(\phi_0)\right)^2}{2}\right\} \qquad (3.4)$$

Similarly, if the AoA distribution is small-Δ uniform distribution which ranges from -Δ to Δ with mean angle Φ_0, the spatial correlation can be derived as

$$\rho(d)=\exp\left(j\frac{2\pi d}{\lambda}\sin(\phi_0)\right)\sin c\left(\frac{2\pi d}{\lambda}\cos(\phi_0)\Delta\right) \qquad (3.5)$$

Equations (3.4) and (3.5) have provided simple generalized formula for spatial correlation and shown that both give good approximations. Another advantage of Equations (3.4) and (3.5) is they have reduced the computation time where the calculation of the spatial correlation originally relies on numerical integration or infinite series expansion. However, as shown in [11], Equations (3.4) and (3.5) cannot approximate well when the mean angle Φ_0 is much larger than 0°, or the standard deviation of the distribution σ becomes higher (or Δ becomes larger in the uniform distribution). That is therefore not favorable because the angular spread of the AoA distribution may become larger in the multiple scattering-rich environment, especially in the indoor environment where MIMO systems can make the best use of their advantages. As a result, in Section 3.1.2, we will further propose the spatial correlation formulation which is suitable for large angular-spread AoA distribution and even arbitrary AoA scenarios.

3.1.2 Spatial Correlation of Arbitrary AoA Scenarios

Uniform distribution is suitable to describe large angular spread AoA in multiple scattering rich environments, so it is an appropriate candidate when we analyze the parameter of the multipath channel model. As mentioned in the previous section, the approximate form of the spatial correlation is presented based on Gaussian distribution which is suitable for small angular spread AoA distribution. However, the approximation may be distorted when the angular spread becomes large, and that is the reason why we would like to suggest a good approximate spatial correlation under the condition of large angular spread. For the uniform distribution, its probability density function is presented as

$$p_{\phi}(\phi) = \frac{1}{2\Delta} \qquad \phi_0 - \Delta \le \phi \le \phi_0 + \Delta \tag{3.6}$$

where Φ_0 is the mean of the given uniform distribution and 2Δ is the range of angles referred to Φ_0. If 2Δ is equal to 2π, the spatial correlation has a closed form and is well-known as the Bessel function; however, for the case that 2Δ is smaller than 2π, the spatial correlation is not a closed form formula and thus the time-consuming numerical integration is needed.

Therefore, we propose a new approximate AoA distribution for the uniform distribution as

$$p_{\phi}(\phi) = \frac{1}{\mathrm{N}} \sum_{\mathrm{n}=1}^{\mathrm{N}} \frac{1}{\sqrt{2\pi}\sigma_n} \exp\left\{ -\frac{(\phi - \phi_n)^2}{2\sigma_n^2} \right\} \tag{3.7}$$

where N is the number of sampling Gaussian distribution, Φ_n is the n-th sampling mean AoA and σ_n is the n-th sampling AoA angular spread. This approximate AoA distribution uses the combination of many small angular spread Gaussian distributions to fit a given large angular spread uniform distribution as shown in Figure 3.1(a). There are three reasons we choose multiple Gaussian distributions to fit the large

angular spread uniform distribution. First of all, Gaussian distribution is a general distribution to describe a small angular spread AoA scenario. Second, the standard deviation of the Gaussian distribution is actually the angular spread of the Gaussian AoA distribution. Finally, that the spatial correlation of small angular spread Gaussian distribution has a generalized approximation formulation is the most important reason we choose as the fitting function of the uniform distribution.

Substitute Equation (3.7) into Equation (3.1), we may represent the spatial correlation as

$$\rho(d) = \frac{1}{\mathrm{N}} \sum_{\mathrm{n}=1}^{\mathrm{N}} \int_{-\pi}^{\pi} \exp(j2\pi \frac{d}{\lambda} \sin(\phi)) \frac{1}{\sqrt{2\pi}\sigma_n} \exp\left\{ -\frac{(\phi - \phi_n)^2}{2\sigma_n^2} \right\} d\phi \quad (3.8)$$

Using the small angular-spread approximate spatial correlation as shown in Equation (3.4), we may finally represent the spatial correlation as

$$\rho(d) = \frac{1}{\mathrm{N}} \sum_{n=1}^{N} \exp\left\{ j \frac{2\pi d}{\lambda} \sin(\phi_n) \right\} \exp\left\{ -\frac{(\frac{2\pi d}{\lambda} \cdot \sigma_n \cos(\phi_n))^2}{2} \right\} \quad (3.9)$$

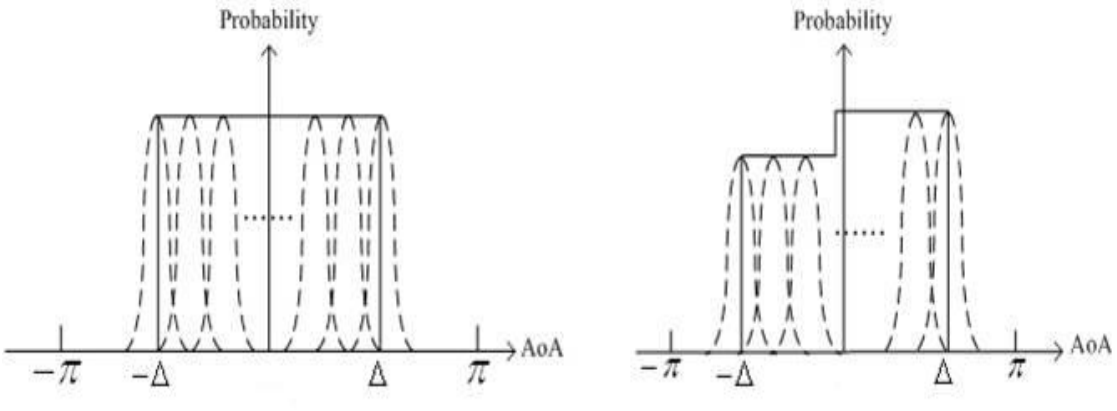

(a) (b)

Figure 3.1 AoA distribution of (a) uniform distribution over $-\Delta$ and Δ and (b) uniform-like distribution. The solid lines are the practical distribution curves while the dash lines are the sampling Gaussian distributions.

The advantage of this approximation is it can be extended to arbitrary AoA scenarios as shown in Figure 3.1(b) as an example. For an AoA distribution which is very complex or cannot be described by a mathematical formula easily, the discretized summation is needed for correlation evaluation. The approximate formulation we propose only samples specific mean AoAs over the distribution and uses the sampling Gaussian distributions to calculate the spatial correlation. Computation time of correlation calculation can thus be saved using the proposed approximation formulation. What should be mentioned is the weighting coefficients of the sampling Gaussian distributions may not equal 1/N and should be modified according to the AoA scenario.

3.1.3 Simulation Results

We first show the performance of 2-D spatial correlation between two ideal sources either by the conventional discretized summation or our approximation formulation. Simulation programs are written in MATLAB® and run on PC with an Intel® Pentium IV 3-GHz CPU. A uniformly-distributed AoA scenario over [-100°,100°] with mean angle 0° is chosen as the benchmark to evaluate the spatial correlation. In order to find a gauge to examine either the discretized summation or the approximation formulation performs correctly, the computation result of the numerical integration is regarded as the closed-form solution.

As from the work in [11], the approximate spatial correlation only fit well with the one calculated in either the closed-form or the discretized manner under the condition of small angular spread. For the value of angular spread larger than 20°, the approximate spatial correlation may perform a less desirable result. Therefore, each of the multiple Gaussian AoA distributions should also be chosen in the manner of small

angular spread, and in our case is 2.5° in the confidence of accuracy. As soon as the angular spread of each sampling AoA distribution is determined, we further make use of the characteristic of Gaussian distribution where the values within two standard deviations from the mean are more than 95 %. The sampling mean AoAs are thus chosen at every 5°, which is two standard deviations from the mean angle.

The correlations calculated by three different schemes in Figure 3.2 share similar curve trend with very little variation. Numerical integration costs more time than the other two schemes as shown in Table 3.1; the main efficiency comparison is made between discretized summation and approximation formulation, and we find that the computation time of approximation formulation is 36% reduced compared to that of discreitized summation. Moreover, of course we can sample more Gaussian distributions for a given arbitrary AoA distribution. However, it will be similar with the calculation using discretized summation and lead to redundant computation time. On the other hand, too few sampling small angular-spread Gaussian distributions are absolutely unable to describe the given arbitrary AoA distribution.

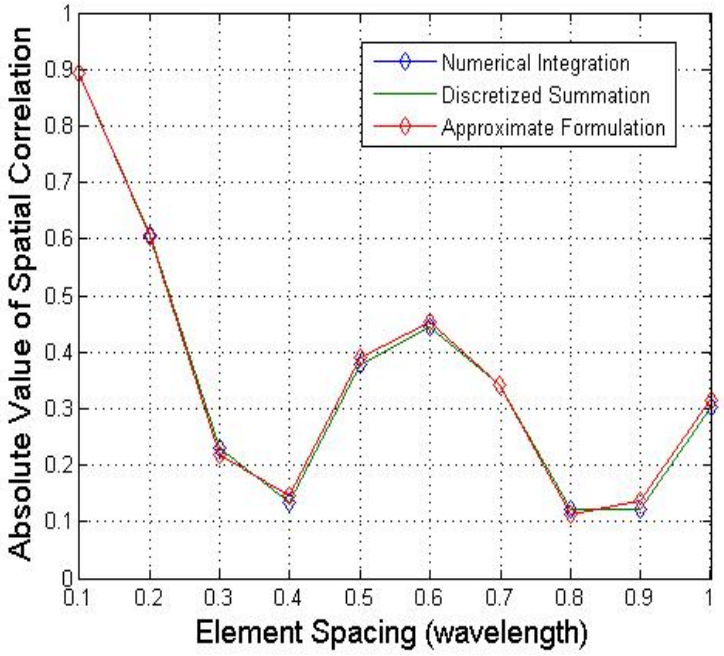

Figure 3.2 Absolute value of spatial correlation using different calculation schemes.

TABLE 3.1 EFFICIENCY COMPARISON OF DIFFERENT SCHEMES IN FIGURE 3.2

Scheme	Computation Time
Numerical Integration	1.266 sec.
Discretized Summation	0.125 sec.
Approximation	0.08 sec.

3.2 2-D Spatial Correlation Formulation Incorporating Antenna Mutual Coupling

3.2.1 Formulation Derivation Incorporating Antenna Mutual Coupling

In Section 3.1, we have discussed the antenna spatial correlation taking AoA distribution into consideration, and introduced our proposed approximate spatial correlation formulation of arbitrary AoA scenarios. Besides AoA distribution, the characteristics of multiple antennas also play an important role in the spatial correlation. In [17], the authors derived an analytical expression for both the mean received power of each antenna and the spatial correlation between antennas with antenna mutual coupling. We therefore would like to combine both our proposed approximate antenna spatial correlation with the spatial correlation which is proposed in [17] to reach a more efficient calculation of the antenna spatial correlation.

Based on the equivalent circuit network model for multiple antenna system in [20], the extension version with incoming waves and load impedances Z_L are shown in Figure 3.3. For closely spaced elements, the coupling matrix is introduced to take mutual coupling effect and load impedances into account. Using the circuit theory, the

coupling matrix is given as

$$C = (z_L + z_A)(Z_L + Z)^{-1} \tag{3.10}$$

where z_L and z_A are the load impedance and antenna self impedance, and Z_L and Z are the load impedance matrix and antenna impedance matrix respectively. One thing which should be reminded is Equation (3.10) is under the assumption that the multiple antenna systems is composed of identical antenna elements and terminated with the same load impedances.

For a dual antenna system, the coupling matrix is assumed as

$$C = \begin{bmatrix} a & b \\ b & a \end{bmatrix} \tag{3.11}$$

where a and b are called self coupling coefficient and mutual coupling coefficient respectively. Different from the deduction in [17], modifications have been made to set up the antennas at both sides of the origin of the axis so that the patterns of the dual antenna system can share the property of symmetry. Consider there is no mutual coupling the dual antenna system, and the received signal vector is given by

$$V^{nc}(\phi) = [g_1(\phi)e^{-j\frac{\tau}{2}} \quad g_2(\phi)e^{j\frac{\tau}{2}}]^T \tag{3.12}$$

where $g_x(\Phi)$ (x=1, 2) is the radiation pattern of the x-th element without mutual coupling, $\tau=2\pi d\sin(\Phi)/\lambda$ is the delay between two neighboring elements, d is the element spacing, λ is the wavelength and Φ is the AoA. If taking mutual coupling into account, we may get the received signal vector as

$$\begin{aligned} V^c(\phi) &= C \cdot V^{nc}(\phi) \\ &= \begin{bmatrix} a \cdot g_1(\phi)e^{-j\frac{\tau}{2}} + b \cdot g_2(\phi)e^{j\frac{\tau}{2}} \\ a \cdot g_2(\phi)e^{j\frac{\tau}{2}} + b \cdot g_1(\phi)e^{-j\frac{\tau}{2}} \end{bmatrix} = \begin{bmatrix} V_1^c(\phi) \\ V_2^c(\phi) \end{bmatrix} \end{aligned} \tag{3.13}$$

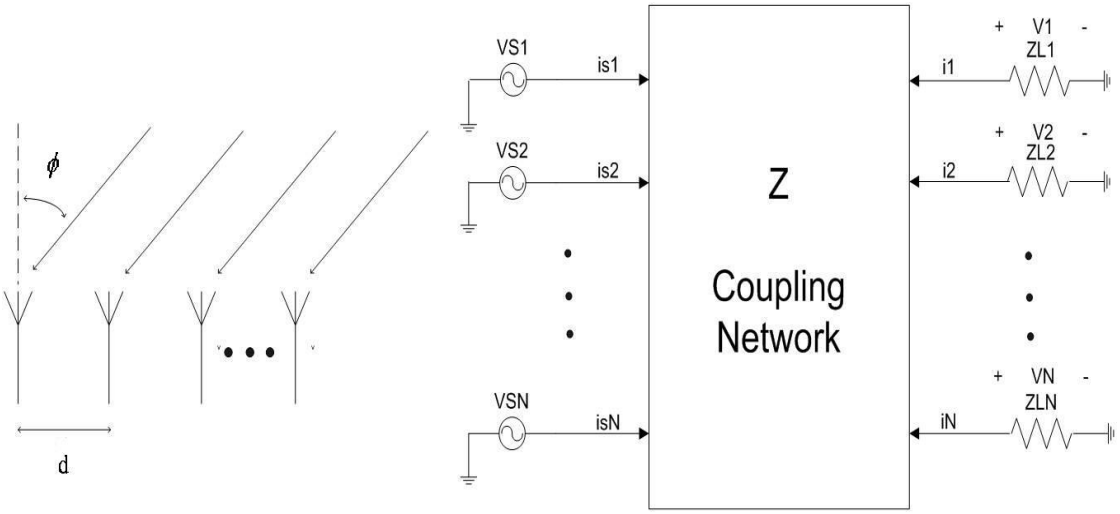

Figure 3.3 Equivalent circuit of the multiple antenna system for receiving mode.

Given the AoA power spectrum distribution is p(Φ), the spatial correlation is therefore shown as

$$\rho_{12}^{mc} = \frac{1}{\sqrt{P_1 P_2}} \int_{\phi} V_1^c(\phi) V_2^{c*}(\phi)\, p(\phi) d\phi \tag{3.14}$$

where

$$P_i = \int_{\phi} \left| V_i^c(\phi) \right|^2 p(\phi) d\phi \tag{3.15}$$

For omnidirectional element patterns without mutual coupling, the spatial correlation is denoted as

$$\rho_{12}^{nmc} = \int_{\phi} \exp\left\{ 2\pi d \sin(\phi)/\lambda \right\} p(\phi) d\phi = R_{real} + jR_{imag} \tag{3.16}$$

which is the same formulation of Equation (3.1). After the deduction, Equation (3.14) can be reduced as

$$\rho_{12}^{mc} = \frac{\left[2\,\mathrm{Re}(c) + \left(1 + |c|^2\right) \cdot R_{real} + j\left(1 - |c|^2\right) \cdot R_{imag} \right]}{\sqrt{\left[1 + |c|^2 + 2\,\mathrm{Re}(c) \cdot R_{real} \right]^2 - 4\left[\mathrm{Im}(c) \cdot R_{imag} \right]^2}} \tag{3.17}$$

where c is the ratio of mutual coupling coefficient b to self coupling coefficient a.

Equation (3.17) separates the element factors, including antenna mutual coupling and AoA scenarios, so that the spatial correlation can be dissected for a more detailed

analysis. Moreover, another advantage is we can combine our proposed approximate antenna spatial correlation with Equation (3.17). That is to say, R_{real} and R_{imag} can be calculated in our proposed approximate formulation and substitute into Equation (3.17) to reach a more efficient calculation of the antenna spatial correlation.

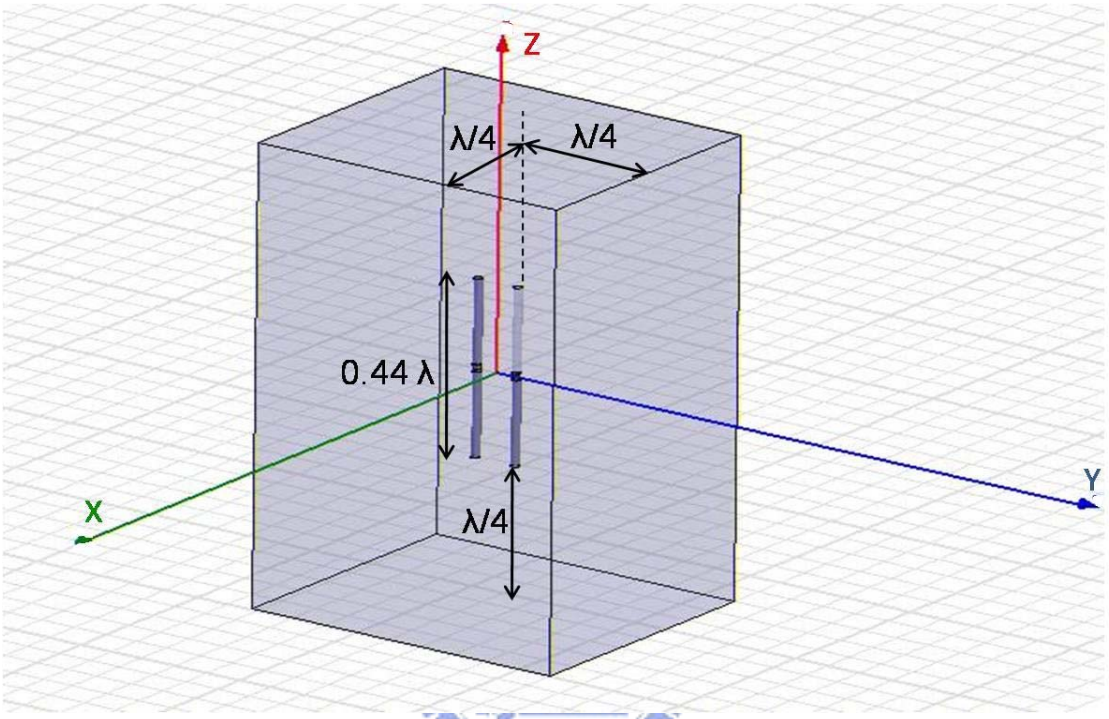

Figure 3.4 HFSS simulation setup of a coupled dipole pair.

3.2.2 Simulation Results

Two parts of simulation results are provided in this section. First of all, we will compare the patterns calculated from the EM simulation tool and calculated from the coupling matrix to verify if the coupling matrix can describe how antenna patterns may distort with mutual coupling effect. Second, we also offer a case study to show how the spatial correlation is affected by mutual coupling. We implement the case study with EM simulation software Ansoft® HFSS, while simulation programs are written in MATLAB® and run on PC with an Intel® Pentium IV 3-GHz CPU.

The likely candidate for the antenna elements is dipole antennas, and Figure 3.4

depicts the design geometry for coupled antenna simulations. The radius of the dipole is λ/100, and the dipole length is tuned to be 0.44 λ in order to make the dipole antenna resonant at the desired central frequency where it is 2.45 GHz in our

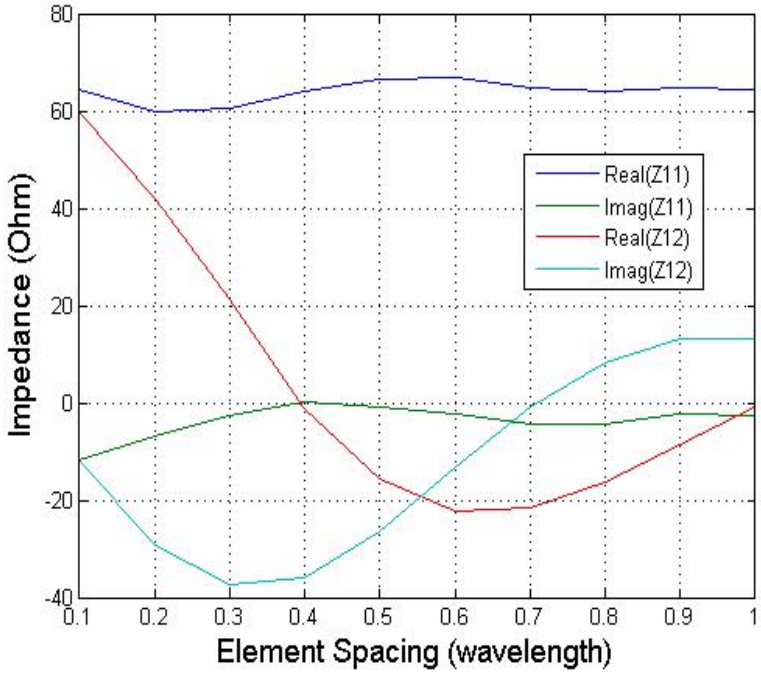

Figure 3.5 The self impedance and mutual impedance ranging 0.1 λ to 1.0 λ.

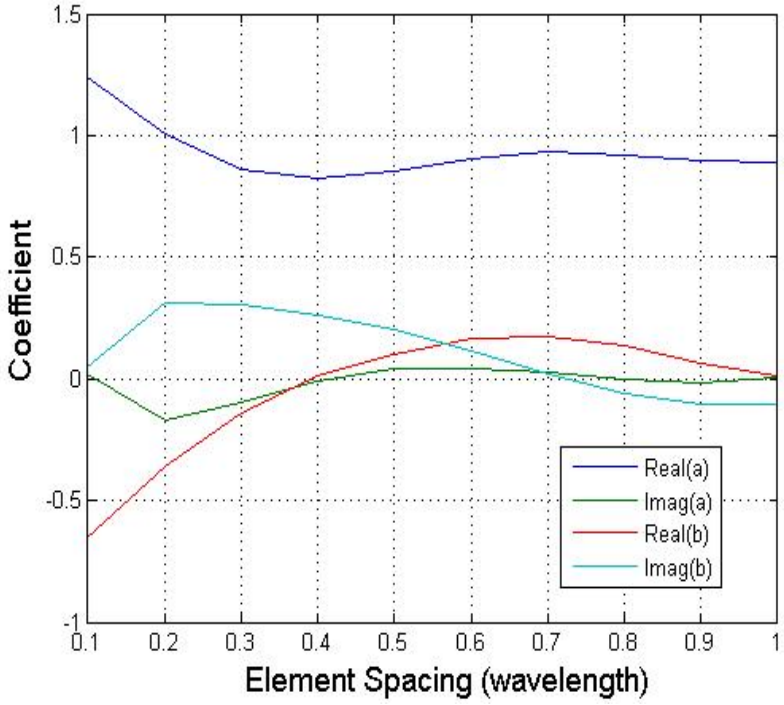

Figure 3.6 Self coupling and mutual coupling coefficient.

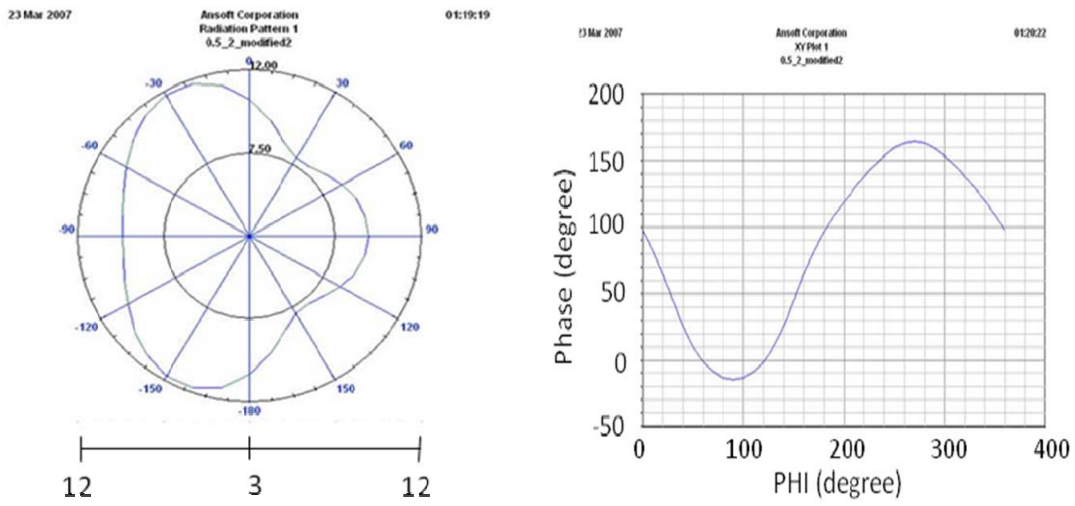

(a) (b)

Figure 3.7 XY-plane E-field pattern computed by HFSS where (a) is the magnitude and (b) is the phase of the pattern.

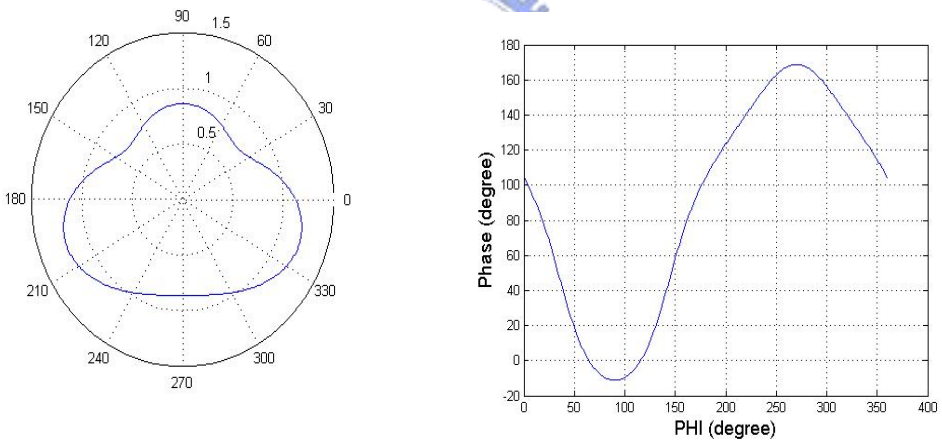

(a) (b)

Figure 3.8 XY-plane E-field pattern computed by the coupling matrix where (a) is the magnitude and (b) is the phase of the pattern.

simulation. With port impedances set to be 50 Ohm, the self impedance and mutual impedance ranging 0.1 λ to 1 λ are shown in Figure 3.5, and the results fit well with those shown in [3]. The self-coupling coefficient and mutual-coupling coefficient in the coupling matrix can be calculated using Equation (3.10) and drawn in Figure 3.6.

With the coupling matrix, the distorted antenna patterns can therefore be computed and compared with those computed from HFSS. Figure 3.7 and Figure 3.8 respectively show the pattern of one antenna branch computed from HFSS and from coupling matrix.

Compare Figure 3.7 and Figure 3.8, and we may find coupling matrix is able to describe the distortion of the antenna pattern, and make sure Equation (3.17) is another candidate of antenna spatial correlation. We further make comparison between antenna spatial correlation in Equation (3.17) and that using traditional discretized summation. A uniformly-distributed AoA scenario over [-180°,180°] is chosen as the benchmark to evaluate the spatial correlation. Moreover, the sampling small angle-spread Gaussian distributions sample their mean angles every 10° with 5° standard deviation for our approximation scheme which will calculate R_{real} and R_{imag} in Equation (3.17). Figure 3.9 shows three antenna spatial correlations. The spatial correlation without mutual coupling actually behaves in the form of Bessel function. What is more important is the calculation results of spatial correlation using different strategies. Observing these two curves, there exists deviation between two calculation strategies. The discretized summation is usually regarded as the reference, and the correlation using Equation (3.17) leads to little lower value than the discretized summation does. This may result from that 1) Equation (3.17) is under the assumption of $g_1(\Phi)=g_2(\Phi)=1$ which is not practical for the explicit for the description of a dipole pattern, 2) discretized summation itself is not the closed form solution, and 3) it is difficult for the coupling matrix to explicitly describe the distortion of the antenna patterns. Figure 3.10 shows two sets of pattern where the deviation of correlation using two strategies is larger and very smaller, including element spacing = 0.3 and 0.8 λ. In order to compare their difference, patterns using two strategies are normalized to their maximum. Obviously from the comparison of these two sets, we

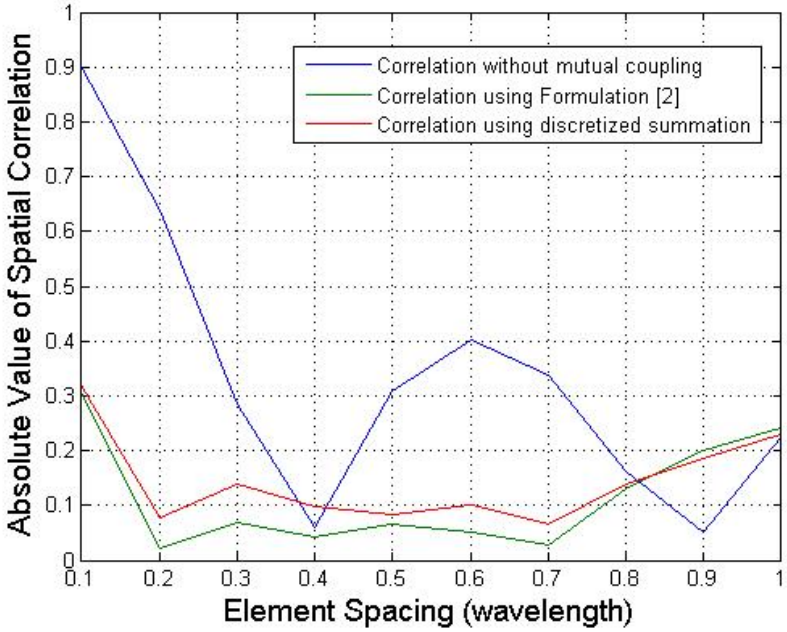

Figure 3.9 Three kinds of absolute value of 2-D antenna spatial correlation.

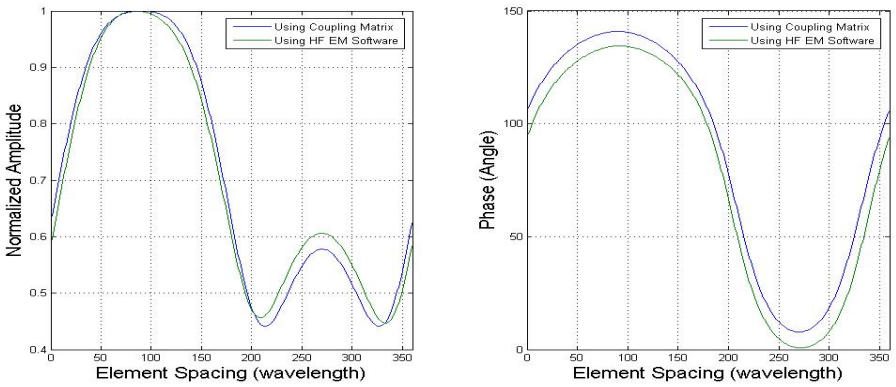

(a)

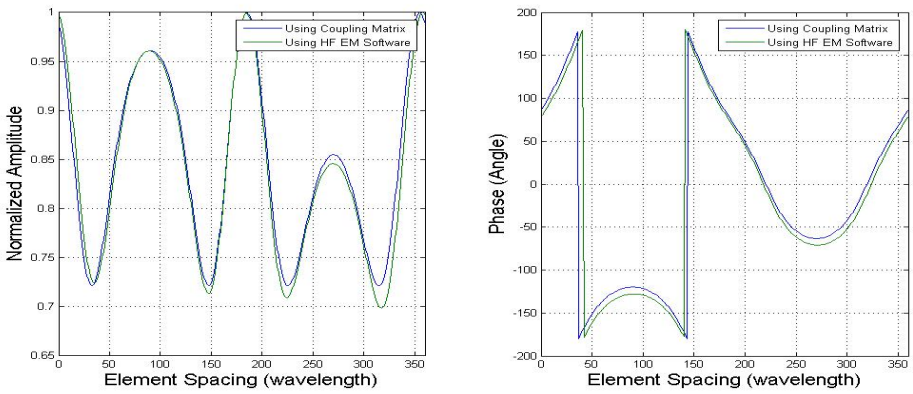

(b)

Figure 3.10 Pattern distortion using coupling matrix and HF EM software where (a) is at element spacing=0.3 λ and (b) at 0.8 λ.

can infer that when mutual coupling is stronger, the pattern becomes more distorted. When the pattern is distorted more dramatically, the coupling matrix is becoming harder to completely describe the fierce distortion, no matter in terms of amplitude or phase. The coupling matrix is originally extracted from the antenna structure, and using the coupling matrix to re-describe the distortion of the antenna patterns may result in the loss of information which the original antenna structure carries. Although it cannot fully describe the distortion and results in deviation of correlation value, the trend of the correlation in Equation (3.17) is still similar with that using discretized summation, and still good for the gauge of the antenna structure before physical implementation.

In terms of the physical meaning of Figure 3.9, it is again shown that mutual coupling can affect and reduce the signal correlation effectively at close antenna spacings just as the conclusion which [17] suggested.

3.3 3-D Spatial Correlation Formulation Incorporating Antenna Mutual Coupling

3.3.1 Formulation Derivation Incorporating Antenna Mutual Coupling

Various definitions of antenna spatial correlation have been introduced in Chapter 2. However, the above definitions have their limited merits. Equation (2.3) is derived under the assumption of the isotropic AoA distribution, but AoA distribution is environment-dependent mentioned earlier. Equation (3.17) in the previous section is another proposal which considers the 2-D antenna pattern and AoA, but antenna

polarization thus is not included in the definition. Equation (2.5) is the most general definition of the spatial correlation; however, compared to Equation (2.3) and Equation (3.17) which both represent spatial correlation in parameterized manner, Equation (2.5) is more computationally complex because 3-D antenna patterns need to be computed individually. Therefore, a parameterized antenna spatial correlation formulation is derived which takes individual 3-D antenna pattern and AoA scenarios into consideration. Essential parameters can be extracted from 3-D antenna patterns and AoA distribution in order to represent the correlation.

Consider two antennas without mutual coupling, and the 3-D received signal vector of the two-element array can be shown as

$$V^{nc} = \begin{bmatrix} g_{\theta,1}(\theta,\phi)\hat{\theta} + g_{\phi,1}(\theta,\phi)\hat{\phi} \\ \left(g_{\theta,2}(\theta,\phi)\hat{\theta} + g_{\phi,2}(\theta,\phi)\hat{\phi} \right) \cdot e^{j\tau} \end{bmatrix} \tag{3.18}$$

where $g_\theta(\theta,\Phi)$ and $g_\Phi(\theta,\Phi)$ are the isolated antenna pattern in theta and phi polarization, and $\tau = 2\pi d\sin(\Phi)\sin(\theta)/\lambda$ is the three-dimensional signal phase difference between two antenna elements. We further incorporate Equation (3.10) into Equation (3.18), and the signal vector can be rewritten as

$$\begin{aligned} V^{c} &= \begin{bmatrix} a g_{\theta,1}(\theta,\phi) e^{-j\tau/2} + b g_{\theta,2}(\theta,\phi) e^{j\tau/2} \\ a g_{\theta,2}(\theta,\phi) e^{j\tau/2} + b g_{\theta,1}(\theta,\phi) e^{-j\tau/2} \end{bmatrix} \hat{\theta} \\ &+ \begin{bmatrix} a g_{\phi,1}(\theta,\phi) e^{-j\tau/2} + b g_{\phi,2}(\theta,\phi) e^{j\tau/2} \\ a g_{\phi,2}(\theta,\phi) e^{j\tau/2} + b g_{\phi,1}(\theta,\phi) e^{-j\tau/2} \end{bmatrix} \hat{\phi} \\ &= \begin{bmatrix} C_{\theta,1}(\theta,\phi) \\ C_{\theta,2}(\theta,\phi) \end{bmatrix} \hat{\theta} + \begin{bmatrix} C_{\phi,1}(\theta,\phi) \\ C_{\phi,2}(\theta,\phi) \end{bmatrix} \hat{\phi} = \begin{bmatrix} C_1(\theta,\phi) \\ C_2(\theta,\phi) \end{bmatrix} \end{aligned} \tag{3.19}$$

where a and b are the self-coupling and mutual coupling coefficient respectively. The spatial correlation between two antennas is then defined as

$$\rho_{12} = \frac{R_{12}}{\sqrt{P_1 P_2}} = \frac{1}{\sqrt{P_1 P_2}} \int_0^{2\pi} \int_0^{\pi} C_1(\theta,\phi) C_2^*(\theta,\phi)\, p_{\theta,\phi}(\theta,\phi) \sin\theta \, d\phi \, d\theta \quad (3.20)$$

where $p_{\theta,\Phi}(\theta,\Phi)$ is the 3-D AoA distribution in theta and phi polarization, and R_{12} and P_i (i=1, 2) are the covariance and the mean received power of the i-th antenna which is defined in Equation (2.6) respectively. R_{12} is first derived as

$$\begin{aligned}
R_{12} &= \int_0^{2\pi}\int_0^{\pi}\left[C_{\theta,1}(\phi,\theta)C_{\theta,2}^*(\phi,\theta)p_\theta(\phi,\theta)\right]\sin\theta d\theta d\phi \\
&\quad + \int_0^{2\pi}\int_0^{\pi}\left[C_{\phi,1}(\phi,\theta)C_{\phi,2}^*(\phi,\theta)p_\phi(\phi,\theta)\right]\sin\theta d\theta d\phi \\
&= |a|^2 \int_0^{2\pi}\int_0^{\pi}\left[\begin{array}{l} c|g_{\theta,2}(\phi,\theta)|^2 + c^*|g_{\theta,1}(\phi,\theta)|^2 \\ +(g_{\theta,2}{}^*(\phi,\theta)g_{\theta,1}(\phi,\theta)e^{-j\tau}) + |c|^2(g_{\theta,1}{}^*(\phi,\theta)g_{\theta,2}(\phi,\theta)e^{j\tau}) \end{array}\right] p_\theta(\phi,\theta)\sin\theta d\theta d\phi \\
&+ |a|^2 \int_0^{2\pi}\int_0^{\pi}\left[\begin{array}{l} c|g_{\phi,2}(\phi,\theta)|^2 + c^*|g_{\phi,1}(\phi,\theta)|^2 \\ +(g_{\phi,2}{}^*(\phi,\theta)g_{\phi,1}(\phi,\theta)e^{-j\tau}) + |c|^2(g_{\phi,1}{}^*(\phi,\theta)g_{\phi,2}(\phi,\theta)e^{j\tau}) \end{array}\right] p_\phi(\phi,\theta)\sin\theta d\theta d\phi \\
&= |a|^2 c \underbrace{\int_0^{2\pi}\int_0^{\pi}|g_{\theta,1}(\phi,\theta)|^2 p_\theta(\phi,\theta)\sin\theta d\theta d\phi}_{A_\theta} + |a|^2 c^* \underbrace{\int_0^{2\pi}\int_0^{\pi}|g_{\theta,1}(\phi,\theta)|^2 p_\theta(\phi,\theta)\sin\theta d\theta d\phi}_{A_\theta} \\
&+ |a|^2 \underbrace{\int_0^{2\pi}\int_0^{\pi}{}^2 g_{\theta,1}(\phi,\theta)g_{\theta,2}{}^*(\phi,\theta)e^{-j\tau}p_\theta(\phi,\theta)\sin\theta d\theta d\phi}_{(Rxx+jRxy)_\theta} \\
&+ |a|^2|c|^2 \underbrace{\int_0^{2\pi}\int_0^{\pi} g_{\theta,2}(\phi,\theta)g_{\theta,1}{}^*(\phi,\theta)e^{j\tau}p_\theta(\phi,\theta)\sin\theta d\theta d\phi}_{(Rxx-jRxy)_\theta} \\
&+ |a|^2 c \underbrace{\int_0^{2\pi}\int_0^{\pi}|g_{\phi,1}(\phi,\theta)|^2 p_\phi(\phi,\theta)\sin\theta d\theta d\phi}_{A_\phi} + |a|^2 c^* \underbrace{\int_0^{2\pi}\int_0^{\pi}|g_{\phi,1}(\phi,\theta)|^2 p_\phi(\phi,\theta)\sin\theta d\theta d\phi}_{A_\phi} \\
&+ |a|^2 \underbrace{\int_0^{2\pi}\int_0^{\pi} g_{\phi,1}(\phi,\theta)g_{\phi,2}{}^*(\phi,\theta)e^{-j\tau}p_\phi(\phi,\theta)\sin\theta d\theta d\phi}_{(Rxx+jRxy)_\phi} \\
&+ |a|^2|c|^2 \underbrace{\int_0^{2\pi}\int_0^{\pi} g_{\phi,2}(\phi,\theta)g_{\phi,1}{}^*(\phi,\theta)e^{j\tau}p_\phi(\phi,\theta)\sin\theta d\theta d\phi}_{(Rxx-jRxy)_\phi} \\
&= |a|^2\left[c(A_\phi + A_\theta) + c^*(A_\phi + A_\theta) + (1+|c|^2)(Rxx_\phi + Rxx_\theta) + j(1-|c|^2)(Rxy_\phi + Rxy_\theta)\right] \\
&= |a|^2\left[2\mathrm{Re}(c)(A_\phi + A_\theta) + (1+|c|^2)(Rxx_\phi + Rxx_\theta) + j(1-|c|^2)(Rxy_\phi + Rxy_\theta)\right]
\end{aligned}$$

P_1 is then deduced by

$$P_1 = \int_0^{2\pi}\int_0^{\pi} \left|C_{\theta,1}(\phi,\theta)\right|^2 p_\theta(\phi,\theta)\sin\theta d\theta d\phi + \int_0^{2\pi}\int_0^{\pi} \left|C_{\phi,1}(\phi,\theta)\right|^2 p_\phi(\phi,\theta)\sin\theta d\theta d\phi$$

$$= |a|^2 \underbrace{\int_0^{2\pi}\int_0^{\pi} \left|g_{\theta,1}(\phi,\theta)\right|^2 p_\theta(\phi,\theta)\sin\theta d\theta d\phi}_{A_\theta} + |a|^2|c|^2 \underbrace{\int_0^{2\pi}\int_0^{\pi} \left|g_{\theta,1}(\phi,\theta)\right|^2 p_\theta(\phi,\theta)\sin\theta d\theta d\phi}_{A_\theta}$$

$$+ |a|^2 c^* \underbrace{\int_0^{2\pi}\int_0^{\pi} g_{\theta,1}(\phi,\theta) g_{\theta,2}{}^*(\phi,\theta) e^{-j\tau} p_\theta(\phi,\theta)\sin\theta d\theta d\phi}_{(Rxx+jRxy)_\theta}$$

$$+ |a|^2 c \underbrace{\int_0^{2\pi}\int_0^{\pi} g_{\theta,2}(\phi,\theta) g_{\theta,1}{}^*(\phi,\theta) e^{j\tau} p_\theta(\phi,\theta)\sin\theta d\theta d\phi}_{(Rxx-jRxy)_\theta}$$

$$+ |a|^2 \underbrace{\int_0^{2\pi}\int_0^{\pi} \left|g_{\phi,1}(\phi,\theta)\right|^2 p_\phi(\phi,\theta)\sin\theta d\theta d\phi}_{A_\phi} + |a|^2|c|^2 \underbrace{\int_0^{2\pi}\int_0^{\pi} \left|g_{\phi,1}(\phi,\theta)\right|^2 p_\phi(\phi,\theta)\sin\theta d\theta d\phi}_{A_\phi}$$

$$+ |a|^2 c^* \underbrace{\int_0^{2\pi}\int_0^{\pi} g_{\phi,1}(\phi,\theta) g_{\phi,2}{}^*(\phi,\theta) e^{-j\tau} p_\phi(\phi,\theta)\sin\theta d\theta d\phi}_{(Rxx+jRxy)_\phi}$$

$$+ |a|^2 c \underbrace{\int_0^{2\pi}\int_0^{\pi} g_{\phi,2}(\phi,\theta) g_{\phi,1}{}^*(\phi,\theta) e^{j\tau} p_\phi(\phi,\theta)\sin\theta d\theta d\phi}_{(Rxx-jRxy)_\phi}$$

$$= |a|^2 \left[(1+|c|^2)(A_\theta + A_\phi) + 2\mathrm{Re}(c)(Rxx_\phi + Rxx_\theta) + 2\mathrm{Im}(c)(Rxy_\phi + Rxy_\theta)\right]$$

P_2 is in the similar form as

$$P_2 = |a|^2 \left[(1+|c|^2)(A_\theta + A_\phi) + 2\,\mathrm{Re}(c)(Rxx_\phi + Rxx_\theta) - 2\,\mathrm{Im}(c)(Rxy_\phi + Rxy_\theta)\right]$$

After the derivation, the 3-D antenna spatial correlation is finally represented as

$$\rho_{12} = \frac{2\mathrm{Re}(c)(A_\theta + A_\phi) + (1+|c|^2)(R_{real,\phi} + R_{real,\theta})}{\sqrt{\left[(1+|c|^2)(A_\theta + A_\phi) + 2\mathrm{Re}(c)(R_{real\phi} + R_{real\theta})\right]^2 - 4\left[\mathrm{Im}(c)(R_{imag,\phi} + R_{imag,\theta})\right]^2}} + \frac{j(1-|c|^2)(R_{imag,\phi} + R_{imag,\theta})}{\sqrt{\left[(1+|c|^2)(A_\theta + A_\phi) + 2\mathrm{Re}(c)(R_{real\phi} + R_{real\theta})\right]^2 - 4\left[\mathrm{Im}(c)(R_{imag,\phi} + R_{imag,\theta})\right]^2}} \quad (3.21)$$

where the lowercase c is the coupling ratio whose value is equal to b/a, A is the expectation value of antenna pattern in terms of the AoA PDF, R_{real} and R_{imag} are the real and imaginary part of spatial correlation for single antenna pattern without mutual

coupling, and the subscript θ and Φ are the value in theta and phi polarization respectively. A, R_{real} and R_{imag} are listed as

$$A = \int_0^{2\pi} \int_0^{\pi} \left| g(\phi,\theta) \right|^2 p(\phi,\theta) \sin\theta d\theta d\phi \tag{3.22}$$

$$R_{real} = \mathrm{Re}(\int_0^{2\pi} \int_0^{\pi} g_1(\phi,\theta) g_2^*(\phi,\theta) e^{-j\tau} p(\phi,\theta) \sin\theta d\theta d\phi) \tag{3.23}$$

$$R_{imag} = \mathrm{Im}(\int_0^{2\pi} \int_0^{\pi} g_1(\phi,\theta) g_2^*(\phi,\theta) e^{-j\tau} p(\phi,\theta) \sin\theta d\theta d\phi) \tag{3.24}$$

What should be mentioned is the polarization of AoA distribution is defined as

$$p_\theta(\phi,\theta) = \frac{1}{1+XPR} \cdot p_{\theta,\phi}(\phi,\theta) \tag{3.25}$$

$$p_\phi(\phi,\theta) = \frac{XPR}{1+XPR} \cdot p_{\theta,\phi}(\phi,\theta) \tag{3.26}$$

where XPR is the abbreviation of cross polarization ratio and we regard θ-polarization is the main polarization while Φ-polarization is the cross polarization. Furthermore, $|\rho_{12}|^2$ is defined as the envelope correlation which describes the effect of mutual coupling on the received power of two branches.

The general correlation formulation like Equation (2.5) takes more computation time because in commercial EM softwares, patterns are generated from the fields distributed on the antennas using near-field-far-field transformation, which is considered a resource-consuming process. By contrast, the proposed spatial correlation extracts c, A and R to perform correlation calculation. That means as long as we can obtain an isolated 3-D antenna pattern and the coupling matrix, the antenna spatial correlation can thus be computed rather than by recording the individual antenna pattern distorted by mutual coupling. Moreover, the parameterized correlation formulation can also be combined with the proposed approximate correlation formulation in Section 3.1 to perform a more efficient correlation calculation.

3.3.2 Simulation Results

We further evaluate the derived 3-D spatial correlation between two 2.45-GHz dipole antennas whose patterns are distorted by mutual coupling effect. The whole HFSS simulation setup is the same as shown in Section 3.2.2, and simulation programs are written in MATLAB® and run on PC with an Intel® Pentium IV 3-GHz CPU. The 3-D AoA scenario for this case study in Figure 3.10 is a 3-D normalized distribution which is an arbitrarily-chosen dual-Gaussian-distributed PDF in phi plane and a 5°-σ Gaussian distribution with mean 90° in theta plane. This scenario is practical in the indoor NLOS channel and similar to the scenario measured in [21]. XPR is assumed to be 0 for this case study. Furthermore, because the approximation formulation in Section 3.1 belongs to 2-D type, the approximate formulation is exploited in phi plane. As for theta-plane AoA distribution, we choose the discretized summation in advantage of its characteristic of small angular spread.

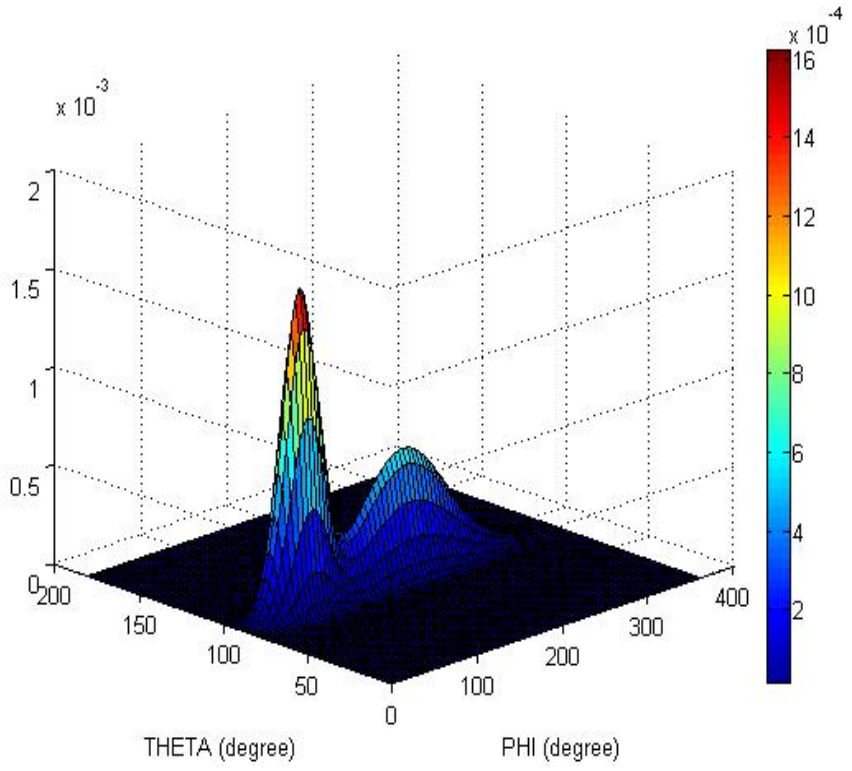

Figure 3.11 The 3-D AoA distribution in Section 3.3.2.

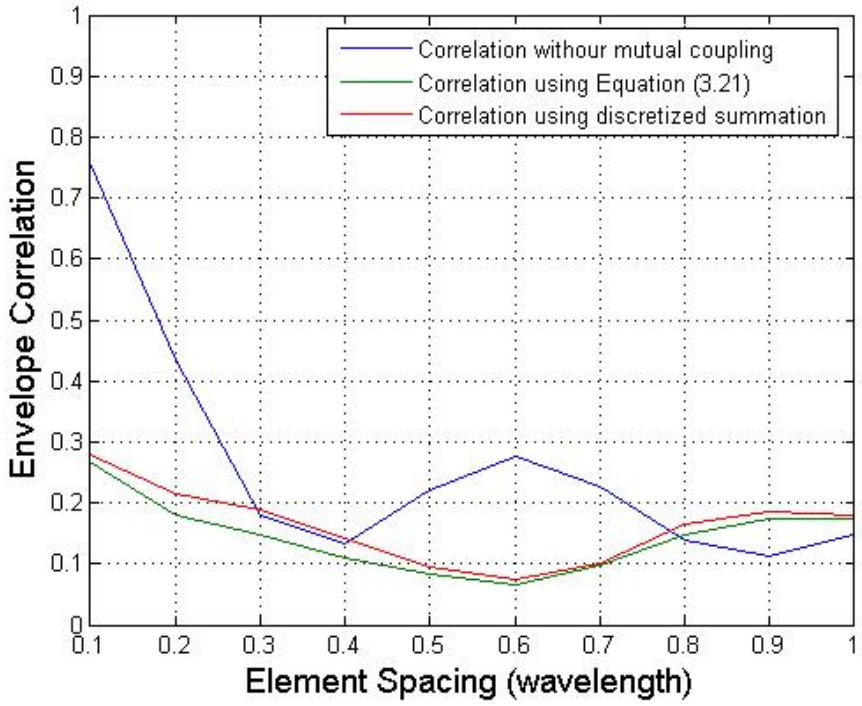

Figure 3.12 Three kinds of absolute value of 3-D antenna spatial correlation.

The computation results of the envelope correlation are shown in Figure 3.12. The correlation values calculated by either conventional discretized summation or Equation (3.21) share similar trend again, and the time computation using approximation formulation is greatly reduced compared to that using discreitized summation. Furthermore, from the observation of Figure 3.11, it can be concluded both the AoA PDF and antenna mutual coupling affect the result of antenna spatial correlation. Given an AoA distribution, antenna spatial correlation tends to decrease with some oscillation as element spacing increases. On the other hand, mutual coupling can effectively reduce the antenna correlation at very close element spacing; however, as the element spacing increases, the mutual coupling will reduce the impact on the pattern distortion, and therefore the spatial correlation will tend to become the same as that without mutual coupling.

For MIMO systems, portable devices containing more than two antennas are also

commonly suggested in the application [22], and a spatial correlation matrix should be introduced to describe the correlation values between different antenna pairs. The multiple-antenna spatial correlation matrix comprises entries which are the spatial correlation values between antenna pairs of the MIMO array. If we further apply the approximate formulation in Section 3.1 and Equation (3.21) to calculation each entry in the matrix, computation time can also be significantly reduced as an additional contribution of our work.

Chapter 4

A New Analysis Strategy of Radiation Efficiency Combined with TARC

In the previous chapter, we have discussed antenna spatial correlation which is regarded as the most important factor in MIMO systems. However, antenna spatial correlation actually matters at the receiver ends for it is the receiving signals that propagate through the multiple scattering rich environments and create the signal diversity and enhance the channel capacity. At the transmit end, because signals are encoded with various coding strategies to combat the multiple scattering effect [19], the antenna correlation is therefore not the top factor we need to take care of when the MIMO systems operate in the transmit mode. It induces us to investigate what actually shows importance in the transmit end.

Radiation efficiency is considered another important factor in MIMO antenna systems, no matter at transmit or receiving mode [15,23]. For the simplicity of analysis, radiation efficiency is usually calculated in transmit mode, and it is exactly what we would like to investigate in this chapter. The basic concept of radiation efficiency has been introduced in Chapter 2, so we continue the texts combined with further investigation of the new analysis strategy of radiation efficiency. In Section 4.1, we introduce the total active reflection coefficient and propose newly-defined radiation efficiency based on TARC. Moreover, the survey of how termination

networks impact on radiation efficiency and spatial correlation is conducted in Section 4.2 to thoroughly compare what kind of termination network works the best when considering both of the two factors.

4.1 The New TARC-Based Radiation Efficiency

4.1.1 Total Active Reflection Coefficient

In general, a multi-polarization antenna is a microwave network with N excitation ports and two radiation ports representing vertical and horizontal polarization states of the radiated fields as shown in Figure 4.1(a) [24]. The generalized scattering matrix of an N-port antenna is an (N+2) by (N+2) matrix. Let us extend this concept to MIMO systems. Each antenna now radiates the RF signals of its own, and the above description should be modified that the general scattering matrix of the N-port antenna is a 2N by 2N matix, which connects all N forward waves at excitation ports and N received waves at radiation ports with N backward waves at excitation ports and N individual radiated signals as shown in Figure 4.1(b). If assuming there is no received waves impinging on the radiation ports, the general scattering matrix is shown as Equation (4.1) where $a_{e,i}$ is the forward waves at excitation ports, $b_{e,i}$ is the reflection waves at excitation ports and $b_{r,i}$ is the radiated waves at radiation ports (i=1 to N).

$$\underbrace{\begin{bmatrix} b_{r,1} \\ \cdot \\ b_{r,N} \\ b_{e,1} \\ \cdot \\ b_{e,N} \end{bmatrix}}_{2N\times 1} = \underbrace{\begin{bmatrix} s_{r1,r1} & \cdot & s_{r1,rN} & s_{r1,e1} & \cdot & s_{r1,eN} \\ \cdot & \cdot & \cdot & \cdot & \cdot & \cdot \\ s_{rN,r1} & \cdot & s_{rN,rN} & s_{rN,e1} & \cdot & s_{rN,eN} \\ s_{e1,r1} & \cdot & s_{e1,rN} & s_{e1,e1} & \cdot & s_{e1,eN} \\ \cdot & \cdot & \cdot & \cdot & \cdot & \cdot \\ s_{eN,r1} & \cdot & s_{eN,rN} & s_{eN,e1} & \cdot & s_{eN,eN} \end{bmatrix}}_{2N\times 2N} \underbrace{\begin{bmatrix} 0 \\ \cdot \\ 0 \\ a_{e,1} \\ \cdot \\ a_{e,N} \end{bmatrix}}_{2N\times 1} \tag{4.1}$$

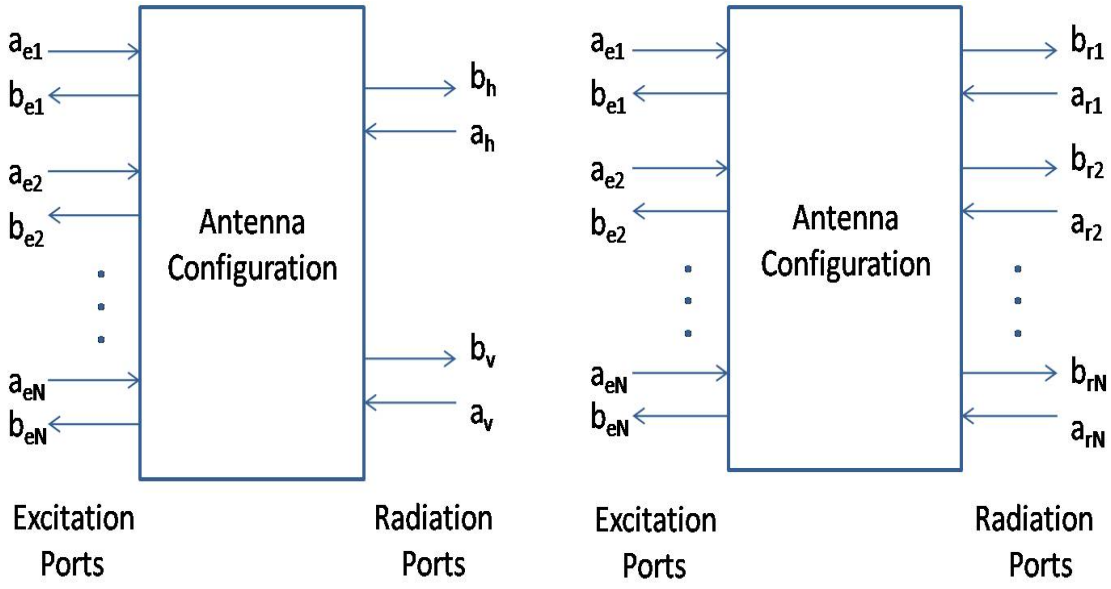

(a) (b)

Figure 4.1 Antenna analysis model for (a) multi-polarization operation and (b) MIMO antenna system.

The radiated power associated with the i-th port, when the other ports are terminated to matched loads and there is no incident wave, is calculated by

$$P_{\text{rad, i-th}} = \left|a_{e,i}\right|^2 \sum_{j=1}^{N} \oint_S \left(s_{rj,ei} s^*_{rj,ei}\right) \cdot ds \tag{4.2}$$

where S is the integral surface enclosing the radiated power of the antenna system. This assumes that the antenna system does not have any loss, and all the power generated by the excitations either radiates or goes through the other ports. A mathematical representation can thus be shown as

$$\sum_{i=1}^{N}\sum_{j=1}^{N}\left(s_{ej,ei} s^*_{ej,ei} + \oint_S \left(s_{rj,ei} s^*_{rj,ei}\right) \cdot ds \right) = 1 \tag{4.3}$$

The radiated power associated with each port normalized to the excitation can be defined as radiation losss, which can thus be calculated based on Equation (4.3) as

$$P_{rad} = \sum_{i=1}^{N}\sum_{j=1}^{N}\left(\int_{S}\left(s_{rj,ei}s_{rj,ei}^{*}\right)\cdot ds\right) = 1 - \sum_{i=1}^{N}\sum_{j=1}^{N} s_{ej,ei}s_{ej,ei}^{*} \tag{4.4}$$

Equation (4.4) shows the physical meaning that how much power turns into radiation can be computed by the total available power minus the power reflected back to the excitation ports for a multiport antenna system.

For a desired port excitation, the total active reflection coefficient (TARC) is defined as the square root of the available power generated from all excitations minus radiated power, divided by the available power as

$$\Gamma_{TARC} = \sqrt{\frac{P_{available} - P_{rad}}{P_{available}}} \tag{4.5}$$

For example, if an N-port antenna is excited at the i-th port and the other ports are connected to termination, the TARC can be calculated as

$$\Gamma_{TARC} = \sqrt{1 - P_{radi\text{-}th}} = \sqrt{\sum_{j=1}^{N}\left(s_{ej,ei}s_{ej,ei}^{*}\right)} \tag{4.6}$$

For multiport excitation, the TARC is therefore in the form of

$$\Gamma_{TARC} = \frac{\sqrt{\sum_{i=1}^{N}\left|b_{e,i}\right|^{2}}}{\sqrt{\sum_{i=1}^{N}\left|a_{e,i}\right|^{2}}} \tag{4.7}$$

The TARC is a real number between 0 and 1. When the value of the TARC is equal to 0, all the delivered power is radiated and when it is 1, all the power either reflects back or goes to the other ports.

4.1.2 Newly-Defined Radiation Efficiency

A general definition of radiation efficiency in multiple antenna systems is also introduced in Section 2.3. Different from the previous definition, we derived the newly-defined radiation efficiency e_{rad} as

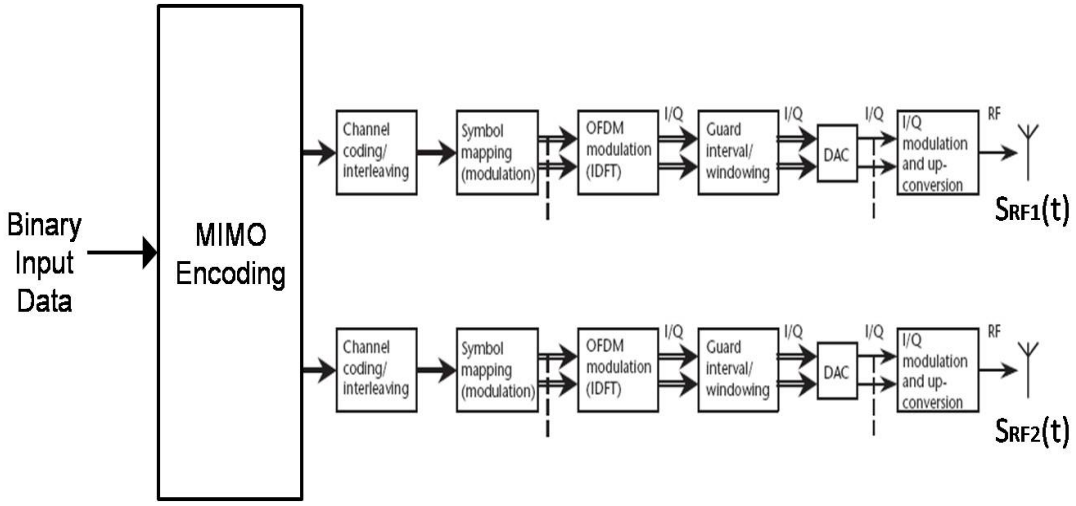

Figure 4.2 MIMO-OFDM system block diagram.

$$\sum_{i=1}^{N} \left|b_{r,i}\right|^2 = \sum_{i=1}^{N} \left|a_{ei}\right|^2 - \sum_{i=1}^{N} \left|b_{e,i}\right|^2 = \sum_{i=1}^{N} \left|a_{e,i}\right|^2 (1 - \Gamma_{TARC}^2) \tag{4.8}$$

$$e_{rad} = \frac{\sum_{i=1}^{N} \left|b_{r,i}\right|^2}{\sum_{i=1}^{N} \left|a_{e,i}\right|^2} = (1 - \Gamma_{TARC}^2) \tag{4.9}$$

It is wondered what is the difference between Equation (4.9) and Equation (2.11). Equation (2.11) is considered the composite power efficiency representation for it includes not only the reflection caused by input mismatch of the excitation port but also the power absorption resulting from the termination at the other unexcited antenna branch. Based on this definition, we may find Equation (2.11) is actually a special case of Equation (4.9). Take a dual-antenna system for example. Equation (2.11) will let one branch of the dual antenna system excite signals and the other terminated with impedance load. While in Equation (4.9), two ports of the antenna system simultaneously excite signal with their own port impedances. That exactly means if we determine the radiation efficiency using Equation (4.9) but with one branch feeding signals of zero amplitude, the analysis result will be the same as that using Equation (2.11). Moreover, if the phase difference between two signals is ± 90°,

Equation (4.9) will have the equivalent result as Equation (2.11) as well.

The most important advantage of the TARC-based definition of radiation efficiency is it takes into account the effect when ports of the multiple antenna system are fed with signals of different phases. TARC is originally developed for signals with various phase delays for multi-polarization operations, and this concept can be further extended to the multiple antenna system [23]. It is well known that mutual coupling causes some portion of signal power within each element to be radiated and absorbed by the other elements. The combination of each antenna port's primary reflected signal with the coupled signals can be constructive or destructive depending on the phase of the component signals. MIMO array efficiency is therefore a function of constructive or destructive signal combination. A more detailed analysis is given as follows. Figure 4.2 represents the MIMO-OFDM system block diagram. Mathematically, the OFDM signal is expressed as a sum of the prototype pulses shifted in the time and frequency directions and multiplied by the data symbols. In continuous-time notation, the k-th OFDM symbol at the n-th transmission branch is given by

$$
\begin{aligned}
&S_{RFn}(t-kT) \\
&= \mathrm{Re}\left\{ w(t-kT) \sum_{i=-N/2}^{N/2-1} \left| x_{i,k,n} \right| e^{j\left(2\pi \left(f_c + \frac{i}{T_{FFT}} \right)(t-kT) + \arg(x_{i,k,n}) \right)} \right\} \\
&\underset{w(t-kT)=1}{\overset{assume}{=}} \sum_{i=-N/2}^{N/2-1} \left| x_{i,k,n} \right| \cos\left(2\pi \left(f_c + \frac{i}{T_{FFT}} \right)(t-kT) + \arg(x_{i,k,n}) \right) \\
&\underset{|x_{i,k,n}|=1}{\overset{assume}{=}} \sum_{i=-N/2}^{N/2-1} \cos\left(2\pi \left(f_c + \frac{i}{T_{FFT}} \right)(t-kT) + \arg(x_{i,k,n}) \right)
\end{aligned}
\tag{4.10}
$$

where T is symbol duration, T_{FFT} is FFT time, N is number of FFT points, f_c is RF central frequency, w(t-kT) is transmitter pulse shaping function, and $x_{i,k,n}$ is digitally modulated signals. We may observe from Equation (4.10) that the RF cosine-modulated signals contain different phase information of the data symbols, which results from the OFDM operation of digitally modulated signals at different transmission branches. This matches the condition that feeding signals of different phases at different antenna elements will result in constructive or destructive performance of radiation efficiency. Therefore, the TARC-based definition of radiation efficiency is considered able to take into account the effect when ports of the multiple antenna system are fed with signals of different phases.

Figure 4.3 and Figure 4.4 represent the radiation efficiency analysis using Equation (2.11) and Equation (4.9) respectively. The whole HFSS simulation setup is the same as in Chapter 3, and simulation programs are written in MATLAB® and run on the PC with an Intel® Pentium IV 3-GHz CPU. Because the phase information of the data symbols depends on many factors, we assume port 1 is excited with unity-amplitude and signal port 2 with exp(jxπ/180°) where x={10°, 20°, …,360°}. This set up contains a range of excitations with unity-amplitude but different phase offset distribution. Compare these two figures, and we may find the phase difference between antenna elements indeed deeply affects the radiation performance. Figure 4.3 only shows -2.7 dB at worst when antenna element spacing is 0.1 λ, but the worst radiation efficiency will be -5 dB which means only about 30 % of the power radiates using the TARC-based radiation analysis.

Another observation from Figure 4.4 is if the antenna element of MIMO is very close to the neighboring element, the radiation efficiency performance will have larger swing margin which means the radiation efficiency may be either very good or very bad at a given close antenna element spacing. The swing margin will become

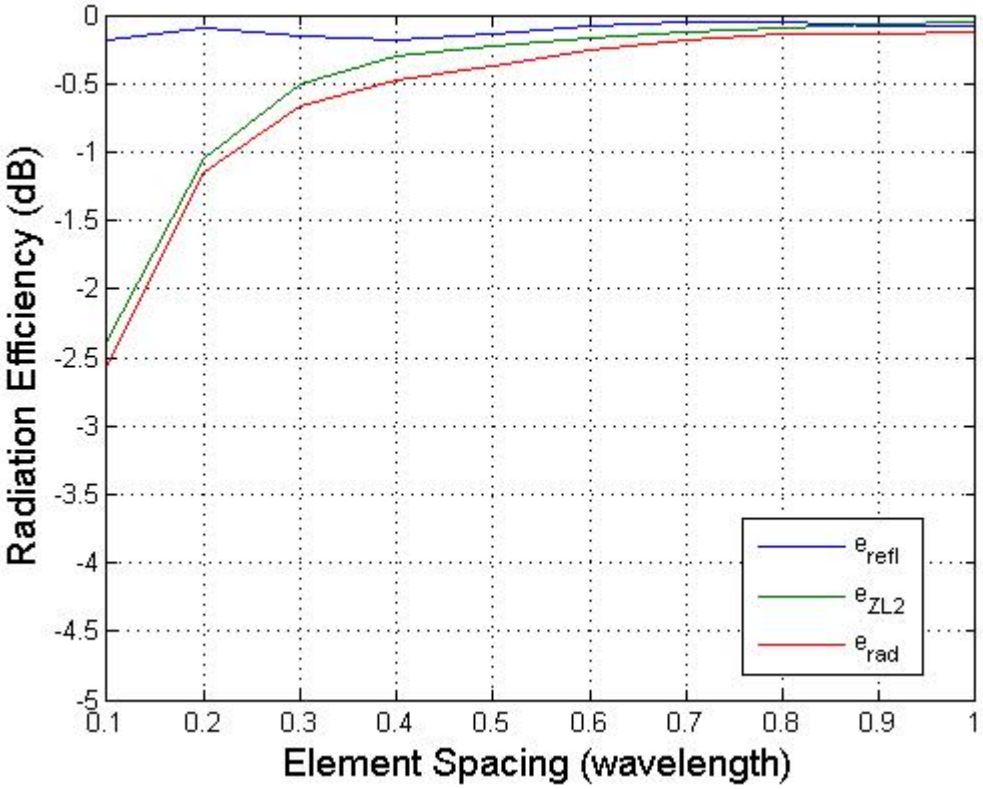

Figure 4.3 Radiation efficiency analysis using Equation (2.11).

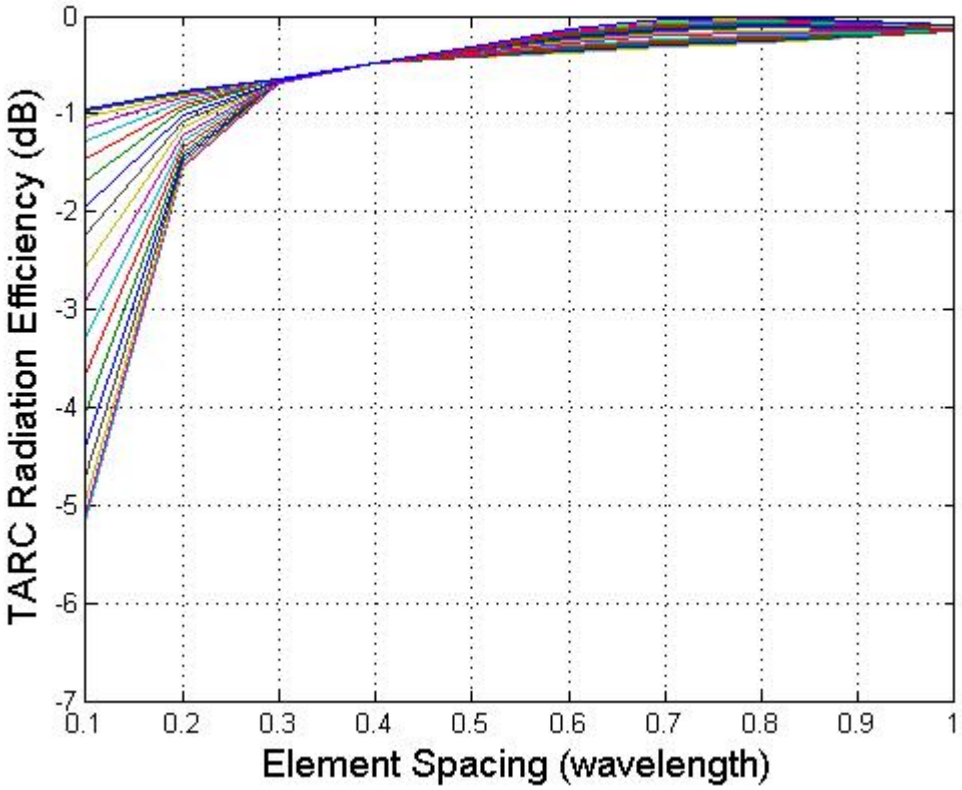

Figure 4.4 Radiation efficiency analysis using Equation (4.9).

smaller as the antenna element spacing increases, where it means the radiation performance would be better and more stable as mutual coupling between antenna elements is less strong.

4.2 Impact of Termination Networks on Radiation Efficiency and Spatial Correlation

In Section 4.1, we have introduced a new analysis strategy combined with TARC. Radiation efficiency is actually a concerned topic when investigating multiple antenna systems especially at transmit mode. On the other hand, antenna spatial correlation actually matters at the receiver ends for it is the receiving signals that propagate through the multiple scattering rich environments and create the signal diversity. This induces our interest to make a composite analysis between antenna spatial correlation and radiation efficiency since a multiple antenna system should be capable of operating in transmit and receiving modes under the same antenna hardware setup. Therefore, we would like to combine the 3-D antenna spatial correlation related to the impedance matrix proposed in [25] and our suggested TARC-based radiation efficiency to complete this survey.

It has been shown that different kinds of termination may pose great impact on both antenna spatial correlation and radiation efficiency in [25] and [15] respectively. In this section, three kinds of termination networks are investigated, including 50-Ohm, self-impedance, and input-impedance termination accordingly.

4.2.1 50-Ohm-Match Termination Network

The simulation setup is shown in Figure 4.5. By two different ways of excitation, we assume there exist two different field solutions respectively. Because two antennas

are identical and, moreover, Z_{S1} (=Z_{L1} at port 2 excitation) and Z_{S2} (=Z_{L2} at port 1 excitation) are identical, the 3-D spatial correlation is obtained as [25]

$$\rho_{ab} = \mathrm{Re}\left\{ \frac{AZ_L - A^* Z_{in}}{\mathrm{Re}[Z_{in}] - |A|^2 \mathrm{Re}[Z_L]} \right\} \tag{4.11}$$

where $A=Z_{21}/(Z_{22}+Z_{L2})$ and Z_{in} is identical to that in Equation (2.10). We will therefore use Equation (4.11) to evaluate the spatial correlation in the following sections as well as in this section.

In this section, $Z_{S1}=Z_{S2}=50$ Ohm first comes as the first case study. Figure 4.6 and Figure 4.7 respectively show the spatial correlation and TARC-based radiation efficiency. Note that port 1 is excited with unity-amplitude signal and port 2 with $\exp(jx\pi/180°)$ where x={10°, 20°,…, 360°} when performing the calculation of radiation efficiency.

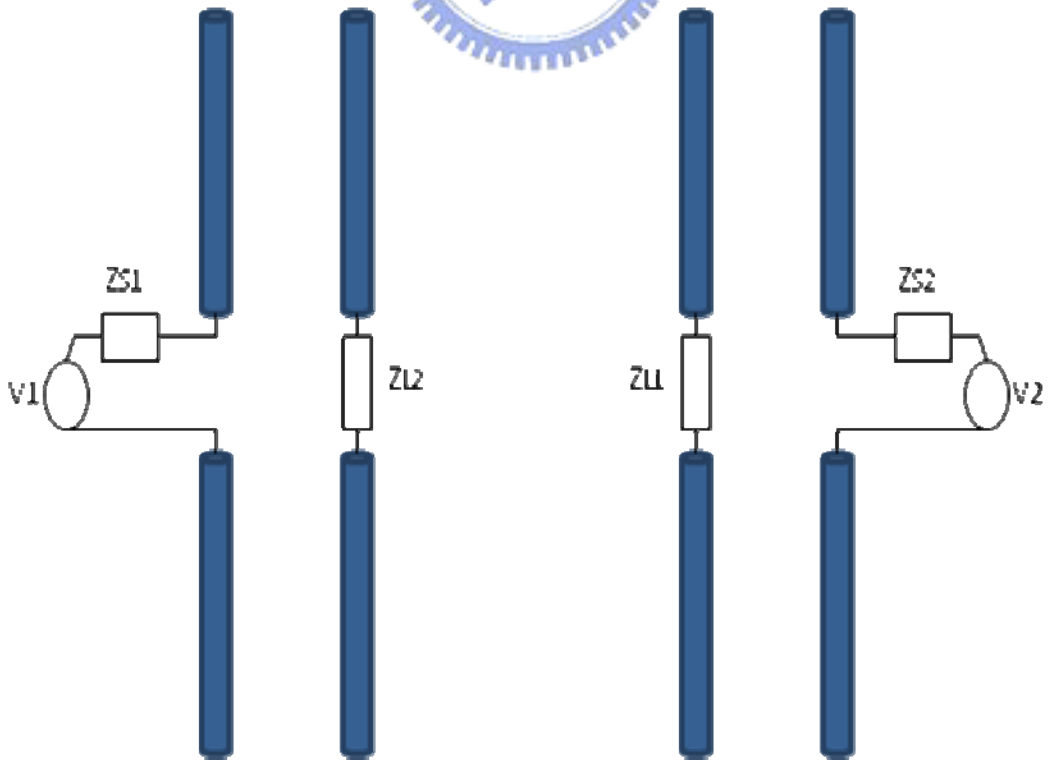

Figure 4.5 Dual antenna system setup with load impedance and source impedance.

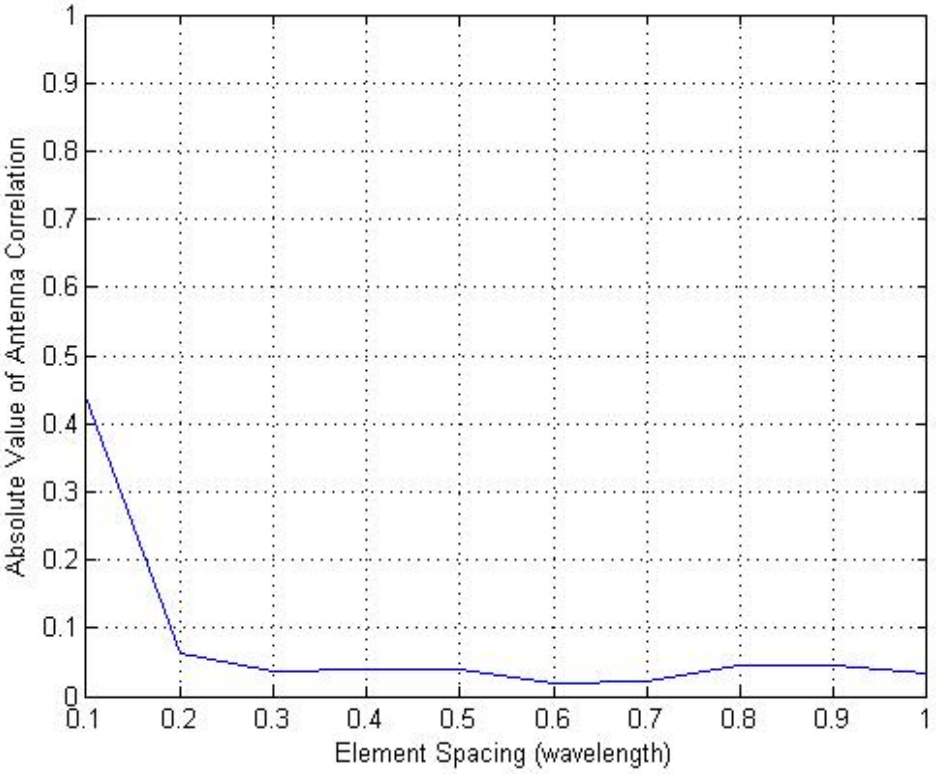

Figure 4.6 Antenna spatial correlation of 50-Ohm termination network.

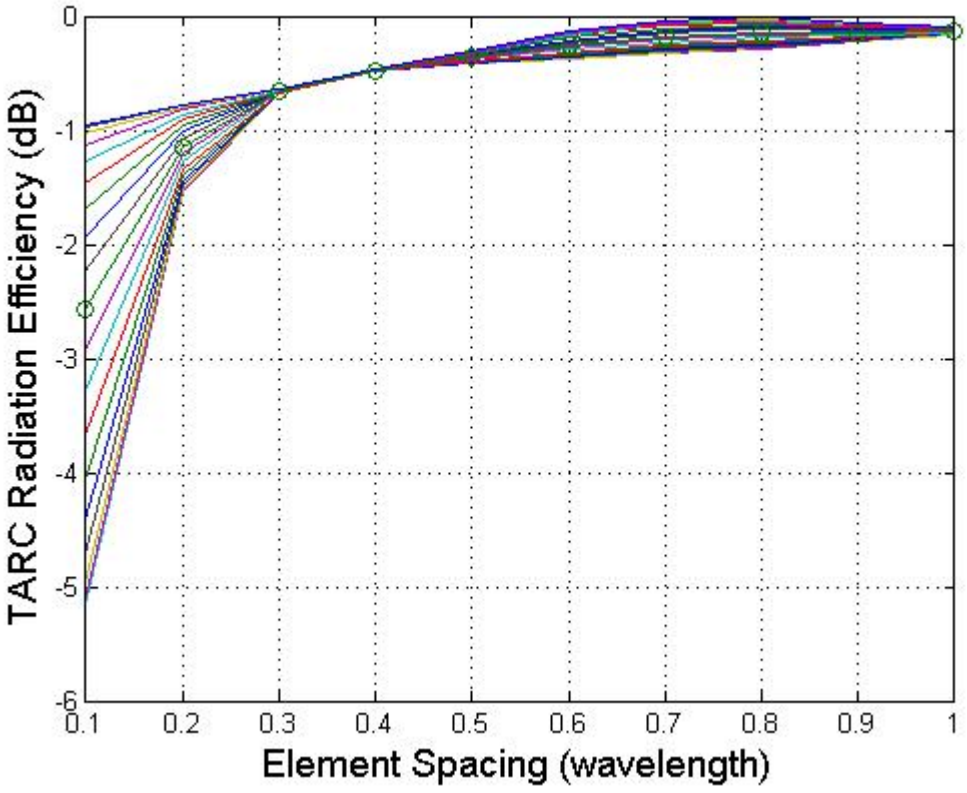

Figure 4.7 TARC-based radiation efficiency of 50-Ohm termination network.

4.2.2 Self-Impedance-Match Termination Network

The same simulation procedure is run like in the previous section. However, this time $Z_{S1}=Z_{S2}=Z_{11}^*$ which is known as the self-impedance source matching (termination) network. What can be mentioned in this simulation procedure is we do not need to re-simulate the dual antenna system which uses 50-Ohm port termination in the previous section to solve the new scattering matrix. By using

$$[S_{new}]=[ZZ_{port}^{-1}+U]^{-1}[ZZ_{port}^{-1}-U] \qquad (4.12)$$

where Z is the impedance matrix, Z_{port} is the diagonal matrix with diagonal terms, and U is the unitary matrix, the new scattering matrix S_{new} can thus be computed and used in calculation of TARC-based radiation efficiency. Figure 4.8 and Figure 4.9 respectively show the spatial correlation and TARC-based radiation efficiency. Again, port 1 is excited with unity-amplitude signal and port 2

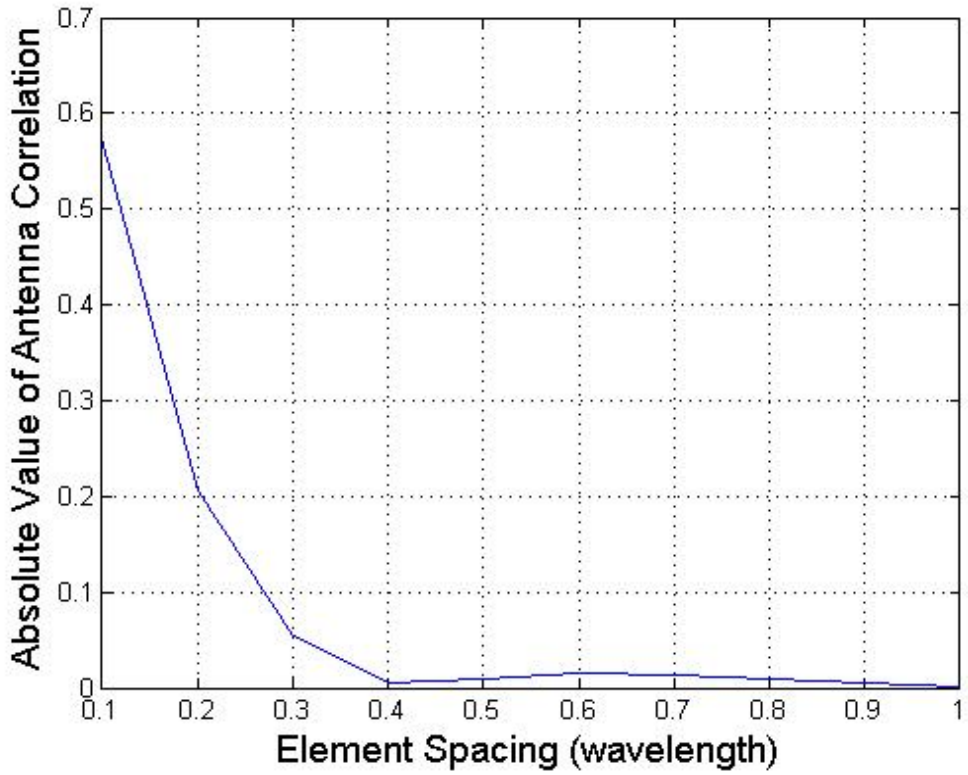

Figure 4.8 Antenna spatial correlation of Z_{11}^* termination network.

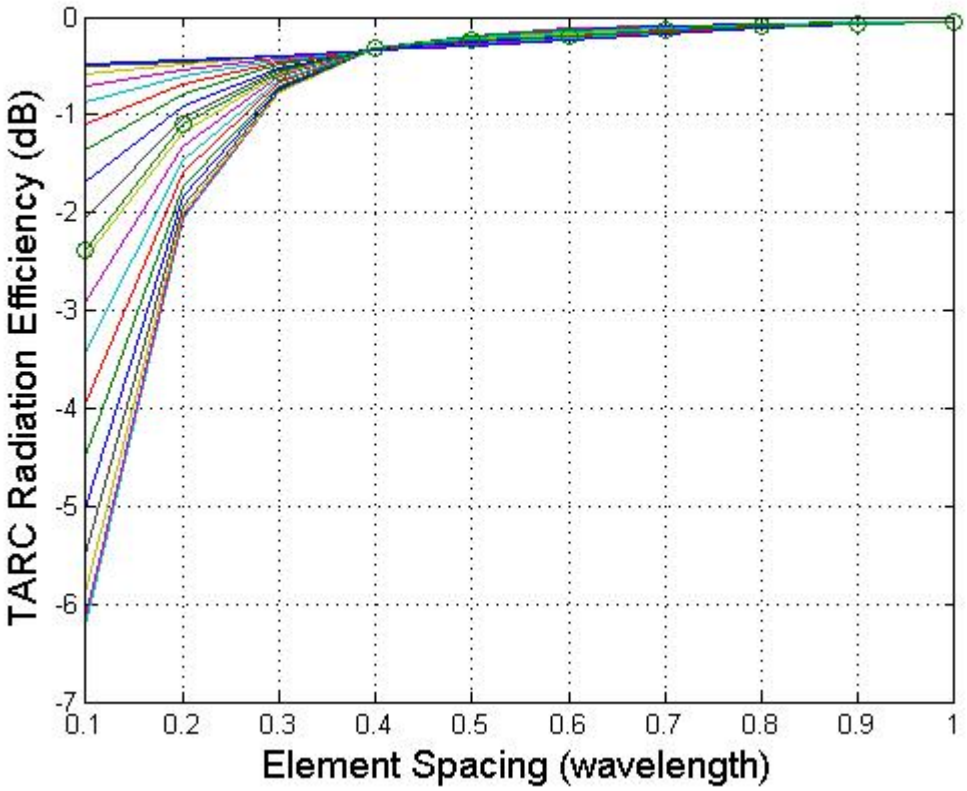

Figure 4.9 TARC-based radiation efficiency of Z_{11}* termination network.

with exp(jxπ/180°) where x={10°, 20°,…, 360°} when performing the calculation of radiation efficiency.

4.2.3 Input-Impedance-Match Termination Network

The input impedance termination network takes into account not only self impedance but also mutual coupling effect. The input impedance termination network means max power transfer from the excitation source to the homologous antenna element physically. Because Z_{S1} is the function of Z_{L2} and vice versa, we may finally derive Z_{S1}, based on Equation (2.10) and $Z_{S1}=Z_{in}$*, as

$$Z_{S1} = \sqrt{R_{11}^2 - R_{12}^2 + X_{12}^2 - \frac{R_{12}^2 X_{12}^2}{R_{11}^2}} + j\left(\frac{R_{12}X_{12}}{R_{11}} - X_{11}\right) \qquad (4.13)$$

where R_{11} and X_{11} are the real and imaginary part of self impedance, R_{12} and X_{12} are the real and imaginary part of mutual impedance. Moreover, the new scattering matrix with Z_{in}* port termination can also be computed and used in calculation of TARC-based radiation efficiency by Equation (4.12). However, one thing should be noticed that when calculating the new scattering matrix, only the real part of the port termination should be substituted into Equation (4.12), and the imaginary part of the port termination should be included into the original antenna impedance matrix. The above operations are mainly for abiding by the sense of max power transfer.

Figure 4.10 and Figure 4.11 respectively show the spatial correlation and TARC-based radiation efficiency.

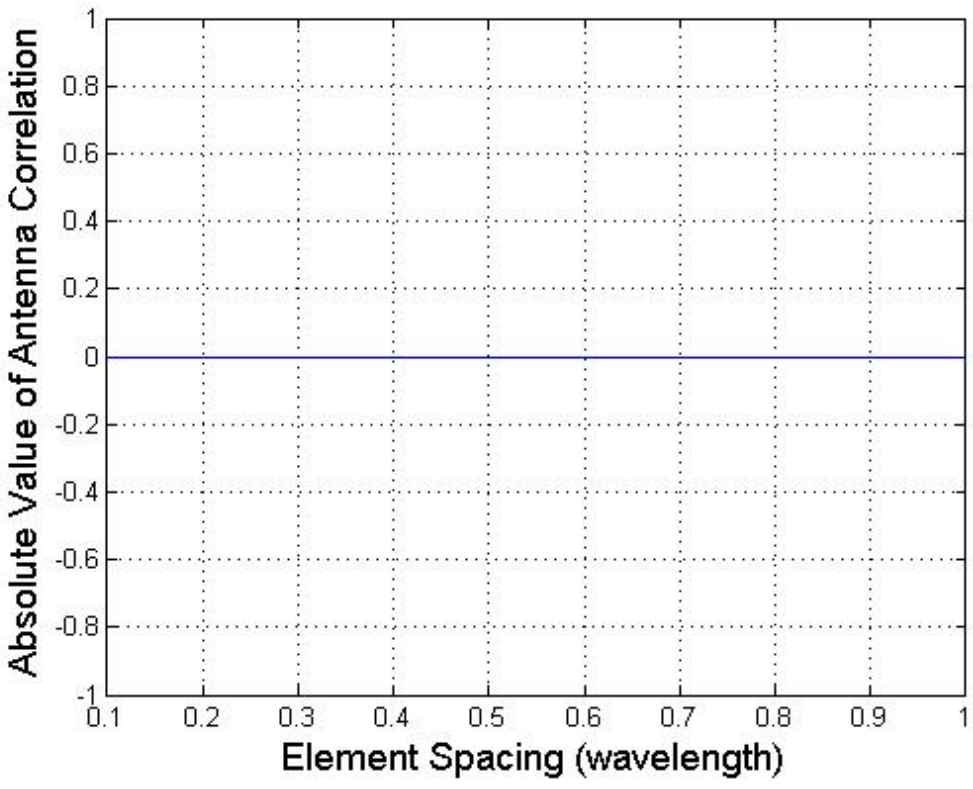

Figure 4.10 Antenna spatial correlation of Z_{in}* termination network.

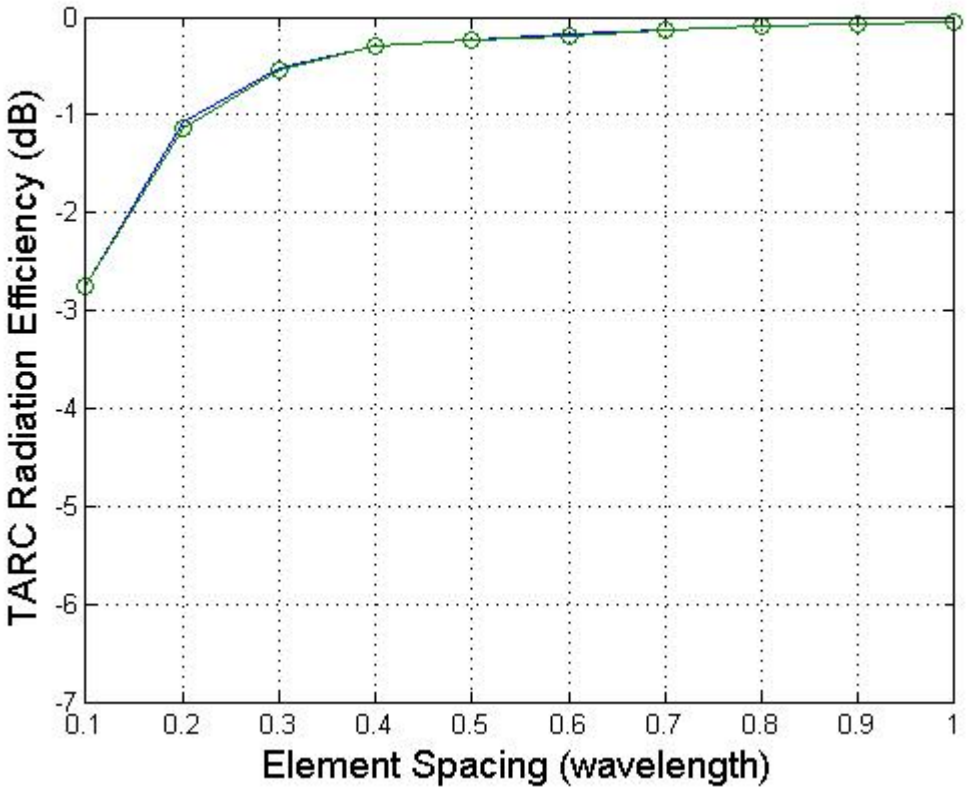

Figure 4.11 TARC-based radiation efficiency of Z_{in}* termination network.

4.2.4 Composite Analysis

Antenna spatial correlation actually matters at the receiver ends for it is the receiving signals that propagate through the multiple scattering rich environments and create the signal diversity. On the other hand, radiation efficiency is actually more important when investigating multiple antenna systems at transmit mode.

We first pay attention to the spatial correlation calculated from three kinds of termination networks in Figure 4.6, 4.8 and 4.10 respectively. Because antenna spatial correlation is actually also dependent on the AoA scenarios as discussed in Chapter 3, we therefore adopt Equation (4.11) as the reference case for it assumes the AoA scenario is 3-D uniform distribution. According to the resulting performance, the input-impedance termination can actually decorrelate the signals between the dual

antenna elements. This agrees well with the result where we let $Z_L=Z_{in}^*$ in Equation (4.11). Since lower correlation between two antenna elements leads to higher signal diversity, an inference can be made that Z_{in}^* case offers the best diversity performance than the other two termination strategies. What's more, the correlation value of 50-Ohm case and Z_{11}^* case will be high (0.45 for 50-Ohm case and 0.57 for Z_{11}^* case) only at element spacing < 0.2 λ. Fortunately, the value will be lower than 0.05 as long as element spacing is larger than 0.3 λ, which can be viewed as decorrelation as well for both cases. A conclusion can be drawn that antenna spatial correlation can be high only at very close antenna element spacing which is about less than 0.3 λ for 50-Ohm case and Z_{11}^* case; in order to decrease the antenna spatial correlation at very close antenna element spacing, Z_{in}^* case can be a good candidate to reach totally decorrelation and high diversity performance.

TARC-based radiation efficiency for three termination cases is shown in Figure 4.7, 4.9 and 4.11 respectively. We first define a parameter called radiation swing margin (RSM) which describes the radiation efficiency swing resulting from the variation of different port-excitation phases. The largest RSM happens when antenna element spacing is 0.1 λ for the first two cases: RSM of 50-Ohm case is about 4 dB which ranges from -1 to -5 dB, RSM of Z_{11}^* case is about 5.5 dB which ranges from -0.5 to -6 dB. Another interesting phenomenon is there are some crossing points occurring in the first two cases. The first crossing point of 50-Ohm and Z_{11}^* cases occur at antenna element spacing =0.4 λ. They can be interpreted that there exists element spacing which is immune from the variation of different excitation phases. A key to the design of MIMO antennas is therefore provided for we may find element spacing beneficial for radiation efficiency which will not be impacted by the random variation of signal excitation phases between ports. Moreover, we can observe RSM would be greatly reduced as element spacing becomes larger, and that can be

interpreted as when the mutual coupling effect is reduced, the radiation efficiency will become much less sensitive to the phase variation of input signal.

Figure 4.11 brings a perfectly good result for there exists no RSM if the termination of the antenna system is chosen to be input-impedance match termination. That exactly represents this kind of termination is immune from the random variation of different port-excitation phases at any antenna element spacing. More explicitly, this is a consequence of the input impedance match termination network taking into account not only self impedance but also mutual coupling effect. This termination technique makes the new scattering matrix composed of very low return loss (S_{11}) and moderate insertion loss (S_{12}) which is dependent on the antenna element spacing, and finally leads to the radiation efficiency which is immune from phase variation. Furthermore, the "o"-marked curve in Figure 4.11 actually represents the conventional radiation efficiency which shares exactly the same trend with the TARC-based radiation efficiency. This again proves the TARC-based radiation efficiency is general for radiation efficiency analysis, and will become the conventional type for the phase-invariant case.

A composite comparison table is shown as in TABLE 4.1. From the comparison, although the first crossing points of 50-Ohm and Z_{11}* cases is at 0.4 λ, the corresponding radiation efficiency is about -0.6 and -0.35 dB, which means at least 8 % of the incident power either reflects back or is absorbed by the load of the adjacent antenna element. On the contrary, since Z_{in}* case results in phase-invariant radiation efficiency, how much power will radiate is then the only concerned topic. However, even if Z_{in}* case is phase-invariant, too close antenna element spacing still results in undesirable radiation performance. For example, when Z_{in}* cases is at 0.1 λ, more than 46 % of input power either reflects back or is absorbed by the load of the adjacent antenna element and not a good solution in the desire of high radiation

efficiency. On the other hand, when Z_{in}* cases is at 0.4 λ, the radiation efficiency has the similar performance with that of Z_{11}* case.

TABLE 4.1 COMPOSITE ANALYSIS TABLE FOR THREE TERMINATION NETWORKS

	First Crossing Point	Efficiency	Correlation
50-Ohm Case	0.4 λ	-0.6 dB	0.05
Z_{11}* Case	0.4 λ	-0.35 dB	0.01
Z_{in}* Case	0.1 λ	-2.75 dB	0

Chapter 5

Concluding Remarks

In the thesis, we proposed two new electromagnetic analysis strategies to evaluate the performance of multiple antenna systems. The first is a new antenna spatial correlation formulation, and the other is a new analysis strategy of radiation efficiency combined with TARC. All the simulation results are provided using a dipole pair as the benchmark.

We first introduced the proposed 2-D approximate spatial correlation formulation of arbitrary AoA scenarios, and derived a 3-D spatial correlation incorporating antenna mutual coupling and AoA scenarios. The new 3-D antenna spatial correlation formulation not only effectively reduces computation complexity without sacrificing much accuracy but also offers a more detailed analysis presented in the parameterized manner, which can be combined with the proposed approximate spatial correlation formulation of arbitrary AoA scenarios.

Secondly, the new suggested analysis of radiation efficiency combined with TARC evaluates how the radiation efficiency may change when the antenna ports excite signals with different phases. Furthermore, the survey of how termination networks impact on radiation efficiency and spatial correlation is conducted based on a dual dipole system. A composite analysis strategy including antenna spatial correlation and the TARC-based radiation efficiency is offered as the gauge of if a

given multiple antenna system is well designed.

Two suggested strategies make a composite analysis between antenna spatial correlation and radiation efficiency since a multiple antenna system operates in both receiving and transmit modes under the same hardware setup of the multiple antenna system. With the proposed analysis strategies, the design of the multiple antenna system can be more efficient and persuasive before physical implementation.

References

[1] D. Gesbert, M. Shafi, D. Shiu, P. J. Smith, and A. Naguib, "From theory to practice: an overview of space-time coded MIMO wireless systems," *IEEE J. Sel. Areas in Commun.*, vol. 21, pp. 281-302, Apr. 2003.

[2] G. J. Foschini and M. J. Gans, "On limits of wireless communications in a fading environment when using multiple antennas," *Wireless Personal Communication*, vol. 6, pp. 311-355, 1998.

[3] C. A. Balanis, *Antenna Theory: Analysis and Design*, New York: Wiley, 1997.

[4] J. Litva, K. Y. Lo, and Titus, *Digital Beamforming in Wireless Communications*, Norwood, MA: Artech House, 1996.

[5] S. M. Alamouti, "A simple transmit diversity technique for wireless communications," *IEEE J. Sel. Areas in Commun.*, vol. 16, pp. 1451-1458, Oct. 1998.

[6] W. C. Jakes, *Microwave Mobile Communications*, New York: Wiley, 1974.

[7] R. H. Clarke, "A statistical theory of mobile radio reception," Bell Syst. Tech. J., vol. 47, pp. 957-1000, 1969.

[8] R. G. Vaughan and J. B. Andersen, "Antenna diversity in mobile communications," *IEEE Trans. Veh. Technol.*, vol. 36, pp. 149-172, no. 4, Nov. 1987.

[9] W. C. Y. Lee, "Effect of correlation between two mobile radio base-station antennas," *IEEE Trans. Veh. Technol.*, vol. 22, pp. 130-140, no. 4, Nov. 1973.

[10] Z. Ying, T. Bolin, V. Plicanic, A. Derneryd and G. Kristensson, "Diversity antenna terminal evaluation," in *Proc. IEEE Antennas and Propag. Soc. Int.*

Symp., Jul. 3-8, 2005, vol. 2A, pp. 375-378.

[11] R. M. Buehrer, "The impact of angular energy distribution on spatial correlation," in *Proc. IEEE 56th VTC Fall*, vol. 2, pp. 24-28, 2002.

[12] W. Wasylkiwskyj and W. K. Kahn, "Theory of mutual coupling among minimum-scattering antennas," *IEEE Trans. Antennas Propag.*, vol. 18, no. 2, pp. 204-216, Mar. 1970.

[13] S. Blanch, J. Romeu, and I. Corbella, "Exact representation of antenna system diversity performance from input parameter description," *Electron. Lett.*, vol. 39, no. 9, pp. 705-707, May 2003.

[14] C. Waldschmidt and W. Wiesbeck, "Compact wide-band multimode antennas for MIMO and diversity," *IEEE Trans. Antennas Propag.*, vol. 52, no. 8, pp. 1963-1969, Aug. 2004.

[15] P. S. Kildal and K. Rosengren, "Electromagnetic analysis of effective and apparent diversity gain of two parallel dipoles," *IEEE Antennas Wireless Propag. Lett.*, vol. 2, pp. 9-13 2003.

[16] H. E. King, "Mutual coupling of unequal length antennas in echelon," *IRE Trans. Antennas and Propag.*, vol. 5, pp. 306-313, Jul. 1957.

[17] X. Li and Z. Nie, "Effect of mutual coupling on performance of MIMO wireless channels," in *Proc. ICMMT 4th International Conference*, pp. 18-21, 2004.

[18] J. Fuhl, A. F. Molisch and E. Bonek, "Unified channel model for mobile radio systems with smart antennas," *IEE Proc. Radar, Sonar Navigation*, vol. 145, no. 1, pp. 32-41, Feb. 1998.

[19] A. E. Zooghby, *Smart antenna engineering*. Norwood, MA: Artech House, 2005.

[20] I. J. Gupta and A. A. Ksienski, "Effect of mutual coupling on the performance of adaptive arrays," *IEEE Trans. Antennas Propag.*, vol. AP-31, no. 5, pp. 785-791, Sep. 1983.

[21] B. K. Lau, J. B. Andersen, G. Kristensson, and A. F. Molisch, "Impact of matching network on bandwidth of compact antenna arrays," *IEEE Trans.*

Antennas Propag., vol. 54, no. 11, pp. 3225-3238, Nov. 2006.

[22] K. L. Wong, C. H. Chang, B. Chen, and S. Yang, "Three-antenna MIMO system for WLAN operation in a PDA phone," *Microwave Opt. Technol. Lett.*, vol. 48, no. 7, pp. 1238-1242, 2006.

[23] D. W. Browne, M. Manteghi, M. P. Fitz and Y. Rahmat-Samii, "Experiments with compact antenna arrays for MIMO radio communications," *IEEE Trans. Antennas Propag.*, vol. 54, no. 11, pp. 3239-3250, Nov. 2006.

[24] M. Manteghi and Y. Rahmat-Samii, "Multiport characteristics of a wide-band cavity backed annular patch antenna for multipolarization operations," *IEEE Trans. Antennas Propag.*, vol. 53, no. 1, pp.466-474, Jan. 2005.

[25] A. Derneryd and G. Kristensson, "Antenna signal correlation and its relation to the impedance matrix," *Electron. Lett.*, vol. 40, no. 7,pp. 401-402, Apr. 2004.